

INVESTIGATION OF SURFACE CONTAMINATION IN A Cu-BASED Al ALLOY
OCCURRING DURING TEM SAMPLE PREPARATION

BY

KELLY M. CLAUNCH

Presented to the Faculty of the Graduate School of
The University of Texas at Arlington in Partial Fulfillment
of the Requirements
for the Degree of

MASTER OF SCIENCE IN MATERIALS SCIENCE AND ENGINEERING

THE UNIVERSITY OF TEXAS AT ARLINGTON

AUGUST 2018

Copyright © by Kelly M. Claunch, 2018

All Rights Reserved

ACKNOWLEDGEMENTS

I would first like to express gratitude to my research advisor, Dr. Choong-Un Kim, for his guidance through this thesis research project. The depth of knowledge and research experience he has shared through this process have been invaluable to me in this undertaking. I would also like to thank him for his patience through the difficult times I have faced in the course of my study, and for always reminding me that nothing is impossible with dedication and hard work. I would also like to extend a special thanks to Dr. Koh and Dr. Hao for reviewing this paper and hearing my thesis defense. Further, I would like to thank the faculty of the MSE Department at UTA for teaching the fundamental science and concepts underlying the field of materials science and engineering in such a way that has challenged me to utilize this knowledge to solve real-world problems.

Additionally, I would like to thank my family and friends for their unwavering support in this endeavor. To my friends in Dr. Kim's research group, thank you for the conversations, laughs, and good times shared. To my parents, thank you for always believing in me, and for always telling me that I can achieve anything in life. To my grandparents, without whom none of this would've been possible, thank you for instilling in me the concept that an education can change a person's life in the best possible ways. Although I will never be able to repay you for your endless generosity in supporting me through this degree, I will be forever grateful.

And last but certainly not least, I would like to thank my boyfriend Tyler for initially encouraging my academic aspirations many years ago. Mostly though, I would like to thank him for sacrifices that he has made in order for me to achieve this dream, and for the patience and limitless supply of support he has given me in the difficult times during this journey. I am so excited to begin the next chapter of our lives together.

August 6th, 2018

ABSTRACT

INVESTIGATION OF SURFACE CONTAMINATION IN A Cu-BASED Al ALLOY OCCURRING DURING TEM SAMPLE PREPARATION

Kelly M. Claunch, M.S. MSE

The University of Texas at Arlington, 2018

Supervising Professor: Dr. Choong-Un Kim

This thesis investigates the nature of surface contamination originating from the jet-polishing process on Cu-6 wt. % Al alloy TEM disks. During previous TEM imaging and diffraction analysis performed by our group, surface contamination particles, roughly 15-60 nm in diameter were observed on the surface of the jet-polished TEM disks. Further, TEM diffraction analysis revealed that the contamination particles are growing epitaxially on the Cu-matrix. HR-SEM was used to characterize the surface contamination in terms of shape, size, composition, and distribution on the surface of the disks. Through extensive HR-SEM imaging, it was found that surface contamination particles are present on the surface of all Cu-6 wt. % Al alloy TEM disks studied in this research. Additionally, a variance in the shape and size of the contamination particles was observed among the different samples and sometimes on individual samples. Low-angle ion milling was chosen as a technique to remove the contamination particles from the surface of the Cu-6 wt. % Al alloy TEM disks. This technique was not successful in removing the particles, and thus the goals of this research moved towards suggesting a mechanism causing the epitaxial growth of the surface contamination in electrolytic conditions. After a review of different epitaxial growth modes, this thesis predicts that a kinetically-controlled 3D growth mode is most likely responsible for the low temperature epitaxial growth

of the contamination particles on the Cu-6 wt. % Al alloy TEM disks. Explaining the variance in shape and size of the contamination particles among the samples was also a goal of this research, and this thesis suggests that this phenomenon could be caused by particle coarsening (Ostwald ripening). Most importantly, the main motivation of this thesis research is to provide awareness for future research and studies to the fact that surface contamination exists on jet-polished TEM samples and can cause deleterious misinterpretation of TEM data.

TABLE OF CONTENTS

ABSTRACT..... iii

LIST OF FIGURES.....viii

CHAPTERS

1. INTRODUCTION..... 1

2. BACKGROUND..... 4

PART I: TEM, JET-POLISHING, AND THIN FILM EPITAXY.....4

2.1 Theoretical Background for TEM.....4

2.1.1 Theoretical Operating Principles of TEM.....4

2.1.2 Image Mode and Diffraction Analysis.....6

2.2 TEM Sample Preparation Techniques.....9

2.2.1 Jet-Polishing Technique.....11

2.2.2 Artifacts Introduced During Jet-Polishing.....16

2.3 Mechanisms Responsible for Surface Contamination
on Cu-Al TEM Disks..... 18

2.3.1 Evidence in Literature..... 20

2.3.2 Mechanisms Describing Epitaxial Particle Growth.....23

PART II: HR-SEM AND ION MILLING.....30

2.4 Background for HR-SEM and Ion Milling.....30

2.4.1 Theoretical Principles and Operating Parameters of HR-SEM.....	30
2.4.1.1 EDS Analysis.....	33
2.4.2 Theoretical Principles and Operating Parameters of Ion Milling...	35
3. EXPERIMENTAL METHODS.....	36
3.1 HR-SEM Characterization.....	36
3.1.1 EDS Analysis and Limitations.....	38
3.2 Low-Angle Ion Cleaning.....	39
3.3 HR-SEM Characterization Post-Ion-Cleaning.....	39
4. RESULTS.....	41
4.1 HR-SEM Characterization of Surface Contamination Particles.....	41
4.1.1 Variance in Shape and Size of the Surface Contamination Particles.....	41
4.2 EDS Analysis Results.....	47
4.3 Comparison of HR-SEM and TEM Images of Contamination Particles.....	49
4.4 HR-SEM Results Post-Ion Cleaning.....	51
5. DISCUSSION, FUTURE RESEARCH, AND CONCLUSIONS.....	55
5.1 Summary of Results and Discussion.....	55
5.1.1 Epitaxial Growth Occurring in an Electrolyte.....	56

5.1.2 Particle Coarsening.....	62
5.2 Future Research and Potential Experiments.....	65
5.3 Conclusions.....	68
REFERENCES.....	70

LIST OF FIGURES

Figure 2.1: Schematic of TEM Components.....	6
Figure 2.2: TEM Bright Field and Dark Field Imaging Modes.....	7
Figure 2.3: Comparison of TEM Set-Up for Imaging Mode and Diffraction Mode.....	8
Figure 2.4: Bright Field Image and Diffraction Pattern of Cu-6 wt.% Al Disk.....	9
Figure 2.5: Image Showing Different Stages of TEM Sample Preparation.....	10
Figure 2.6: Schematic of the Jet-Polishing Process.....	12
Figure 2.7: I-V Curve for Jet-Polishing Process.....	14
Figure 2.8 Layers Formed During Jet-Polishing.....	14
Figure 2.9 Polishing in Plateau Region of Jet-Polishing I-V Curve.....	16
Figure 2.10: Comparison of HR-SEM Image of Contamination Particles with TEM Image from Literature Showing Artifacts from Jet-Polishing on a Ni-Fe-Al Ribbon...	18
Figure 2.11: Comparison of HR-SEM Image of Contamination Particles with SEM Image From Literature Showing Contamination Particles on Electropolished Al-Cu TEM Disk.....	23
Figure 2.12: Diagram Showing Thermodynamically-Driven Epitaxial Growth Modes.....	25
Figure 2.13: Diagram Showing Kinetically-Driven Epitaxial Growth Modes.....	26
Figure 2.14: Diagram Showing Mechanism of Step-Flow Epitaxial Growth Mode.....	27

Figure 2.15: Diagram Showing Mechanism of Layer-by-Layer Epitaxial Growth Mode.....	28
Figure 2.16: Schematic of SEM Components.....	31
Figure 2.17: Diagram Showing Difference Between Back Scattered and Secondary Electrons.....	32
Figure 2.18: Diagram Showing Principles of Characteristic X-Rays.....	34
Figure 2.19: Schematic of Ion Milling Machine.....	35
Figure 3.1: HR-SEM Image Showing Area of Interest on a Cu-6 wt.% Al TEM Disk.....	37
Figure 3.2: Diagram Showing the Sample Depth of Various Signals Generated by Electron Beam in SEM.....	39
Figure 4.1: HR-SEM Images of Cu-6 wt.% Al TEM Samples.....	42
Figure 4.2: AFM Image from Literature Showing the Coarsening of Epitaxially Grown Islands Over Time.....	45
Figure 4.3: Etching of High Density Crystallographic Planes.....	46
Figure 4.4: EDS Spectrum Results.....	47
Figure 4.5: EDS Mapping Results.....	48
Figure 4.6: Comparison of HR-SEM and TEM Bright Field Images of the Cu-6 wt.% Al TEM Samples.....	49

Figure 4.7: Comparison of HR-SEM Images of Surface Contamination Particles Before and After Ion Milling was Performed.....51

Figure 5.1: DMG-Controlled Epitaxial Growth.....59

Figure 5.2: HR-SEM Images of Surface Contamination on Cu-6 wt.% Al vs. STM of DMG Growth of Cu on Au.....61

Figure 5.3: Illustration Showing Particle Coarsening.....62

Figure 5.4: Free Energy vs. Composition Plot for Gibbs-Thompson effect.....64

CHAPTER I

INTRODUCTION

Transmission electron microscopy (TEM) is a powerful tool in materials characterization and analysis. Using transmitted electrons as probes, TEM makes it possible not only to study the surface characteristics of a material, but also to investigate its crystal structure and defects. However, because TEM samples must be electron transparent, with a thickness of approximately 30-50 nm in the area of interest, TEM sample preparation is often a difficult task. Several methods exist for thinning TEM samples, and the method chosen is dependent on the type of material. One commonly used technique for thinning metals and alloys for use in TEM is electropolishing, of which jet-polishing is a variation. As is possible with many other preparation methods, the process of electropolishing can sometimes produce artifacts on the TEM sample surface. This thesis specifically investigates surface contamination occurring during jet-polishing in a Cu-6 wt. % Al alloy [1-3].

In previous experiments, several samples of a Cu-6 wt. % Al were thinned for use in TEM using the jet-polishing technique. TEM images showed small particles, roughly spherical in shape and approximately 15-60 nm in diameter, on the surface of the samples. Additionally, TEM diffraction analysis revealed what initially appeared to be precipitates distributed epitaxially on the Cu matrix. The conclusion of these findings was that the particles seen on the TEM images were not precipitates, but rather surface contamination occurring during the jet-polishing process due to redeposition.

The first goal of this research was to further investigate the shape, size, and composition of the contamination particles present on the surface of the Cu-6 wt. % Al TEM disks. For this

additional imaging, high-resolution scanning electron microscopy (HR-SEM) was chosen due to the nanometer-scale size of the particles. The HR-SEM images showed that, although there is some variation in the shape and size of the particles among different samples, this surface contamination is present on all samples examined in this research. Upon comparison, the shape and size of the particles seen in the HR-SEM images matches well with that of those seen in the original TEM images.

After thorough imaging with HR-SEM, the next step of this research was to find a technique for removing the particles. For this task, ion milling was chosen. Usually, ion milling is a technique that is used for thinning non-conductive samples for use in TEM. The sample is bombarded with high energy ions that sputter material from the surface, thus thinning the sample. Thinning samples for use in TEM using ion milling is a time-consuming process, taking up to several hours depending on the sample material and the desired thickness [2]. However, if used for a short time, such as a few minutes, ion milling can be used to sputter contamination from the surface of the sample without thinning it. After ion milling, additional HR-SEM images were taken to determine if ion milling removed the contamination from the surface of the samples. Comparison of HR-SEM images taken before and after ion milling was performed showed that the surface contamination was not removed during the experiment.

Because ion milling was unsuccessful in removing the contamination particles from the surface of the samples, one of the most important goals of this research aims to identify possible mechanisms by which surface contamination effects occur during jet-polishing and specifically how the particles are growing epitaxially on the sample surface in the Cu-6 wt. % Al alloy. Several studies note surface contamination issues in electropolished TEM alloy disks and suggest possible techniques, some of which are reported to be successful, for removing the surface

contamination. However, none of the studies provide an explanation as to why surface contamination is occurring during electropolishing or mention that the surface contamination observed was growing epitaxially on the surface of the disks. A section of this thesis will discuss the findings of other studies which mention surface contamination due to jet-polishing and attempt to identify a possible mechanism as to why it is occurring. Additionally, various thin film epitaxial growth modes are discussed with the goal of suggesting a mechanism by which the surface contamination particles are growing epitaxially.

For accurate results in areas such as diffraction analysis and compositional surface analysis, the characteristics of TEM samples should reflect the characteristics of the bulk material from which they are prepared. The presence of surface contamination on prepared TEM samples is not representative of the bulk sample and could cause inaccurate conclusions during TEM data analysis. Also complicating this issue and possibly contributing to erroneous conclusions is the fact that it can often be difficult to distinguish surface contamination from true microstructure. Thus, the potential deleterious effects of misinterpreted TEM data caused by surface contamination occurring during jet-polishing warrant the further investigation into this phenomenon that is presented in this thesis.

CHAPTER II

PART I: TEM, JET-POLISHING, AND THIN FILM EPITAXY

2.1 Background for TEM

Since this thesis research is based on observations from previous TEM experiments and analysis performed on the Cu-6 wt. % Al alloy disks, a brief background on TEM will be given in this section, including theoretical operating principles and a discussion about the different kinds of image and analysis modes that are possible with TEM.

2.1.1 Theoretical Operating Principles of TEM

TEM creates an image of a sample by transmitting a high energy beam of electrons through the sample, which then produces an image of the sample on a phosphor screen or CCD. TEM is such a powerful tool because it allows resolution as small as 0.1 nm by utilizing the wave-particle duality of electrons. All particles can be described as waves, and this concept is represented mathematically in the expression for de Broglie wavelength [3]. The de Broglie wavelength is given by:

$$\lambda_{electron} = \frac{hc}{pc} = \frac{hc}{\sqrt{KE^2 + 2 KE m_o c^2}}, \text{ where:}$$

$$hc = 1240 \frac{eV}{nm}$$

$$m_o = \text{rest mass of electron} = .511 \text{ MeV}$$

$$KE = \text{energy of electron beam (100 – 300 keV in TEM)}$$

By comparing the wavelength of the visible light used to generate images in optical microscopes, around 400-700 nm, with the de Broglie wavelength of high energy electrons, between .0009-.004 nm, it is evident why the electrons utilized in in TEM are able to resolve images at significantly higher magnifications than the visible light photons in optical microscopes. Because the de Broglie wavelength of the electrons used in TEM is significantly smaller than both the diameter of an atom and the distance between atoms in a crystal structure, the electrons are not only able to resolve surface images at the atomic scale, but also to extract information about the crystal and defect structure of the material [3].

A typical TEM uses an electron emission source and several different lenses to create the high energy electron beam which will probe the sample. To create electrons, the electron gun, fitted with a tungsten filament or single crystal LaB₆ filament, is connected to a high voltage source of around 100-300 keV. When current is applied to the electron gun, the filament begins to produce electrons. The electron beam is then accelerated into a vacuum chamber and is focused by electromagnetic lenses [3]. A schematic of a typical TEM is shown in Figure 2.1.

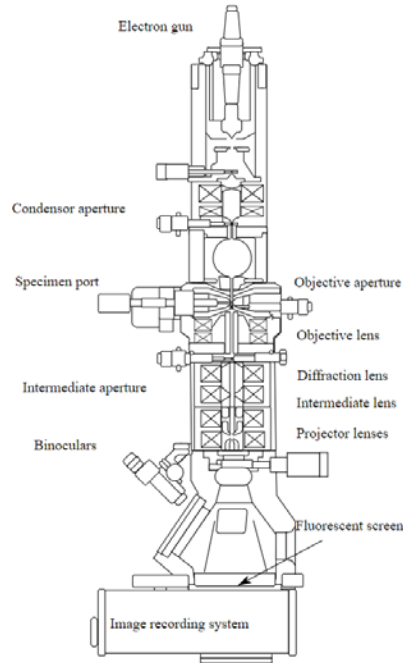


Figure 2.1 [33]

2.1.2 Image Modes and Diffraction Analysis

With TEM, it is possible to use two operational modes, image mode and diffraction mode, to obtain different information about the sample. Further, image mode can produce two different types of images, bright field images (BF) and dark field images (DF). For both BF and DF imaging modes, the objective aperture is inserted into the back focal plane of the objective lens. In BF imaging mode, only the central beam is allowed to pass through the objective aperture, while diffracted beams are blocked. As the electrons interact with the sample, the beam signal will be weakened in thicker areas of the sample, or in areas containing heavier atoms. In the final image, the areas of the sample where the electron beam signal was weakened will appear darker in contrast to areas of the sample where the beam was able to easily pass through the sample. Conversely, DF imaging mode allows diffracted beams to pass through the objective aperture while blocking the intense central beam. In DF imaging mode, structures in the sample

interacting with the diffracted beams will appear bright, while features of the sample that would have otherwise been illuminated by the intense central beam will appear dark. [3-4]. A schematic showing the objective aperture for BF and DF imaging modes is shown in Figure 2.2.

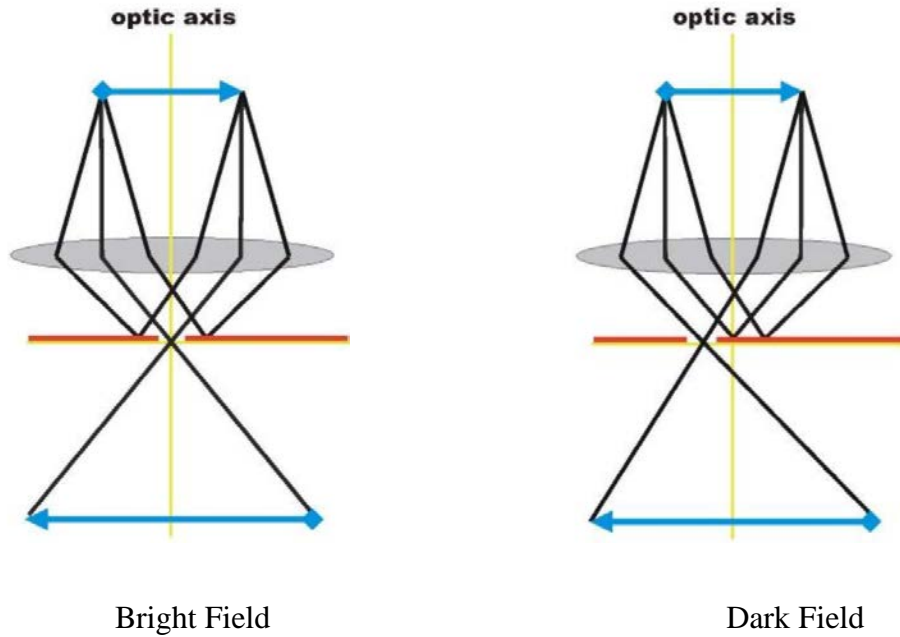


Figure 2.2 [34]

The second type of TEM operation mode is diffraction mode, also referred to as selected area diffraction (SAD), from which the user can gain valuable information about the crystal structure of the sample. In diffraction mode, the objective aperture is removed from the TEM, and a selective aperture lens is placed close to the intermediate lens. Without the objective aperture, all beams are allowed to pass through the sample. The purpose of the selected aperture is to allow the user to focus on a specific area of the sample from which the diffraction pattern will be obtained [3-4]. A schematic showing the difference in TEM components for imaging mode and diffraction mode is shown in Figure 2.3.

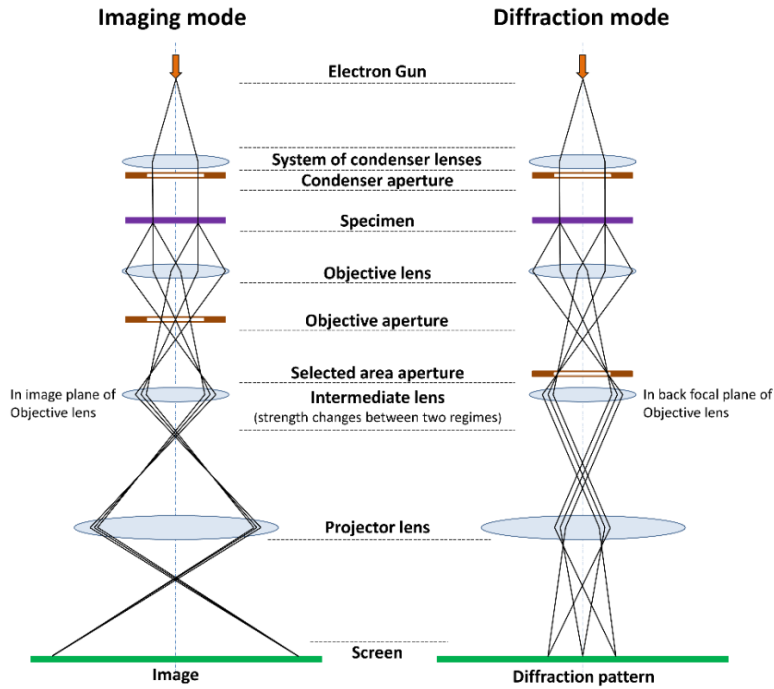
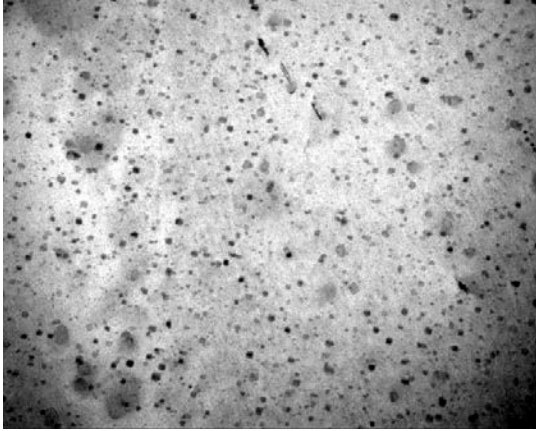
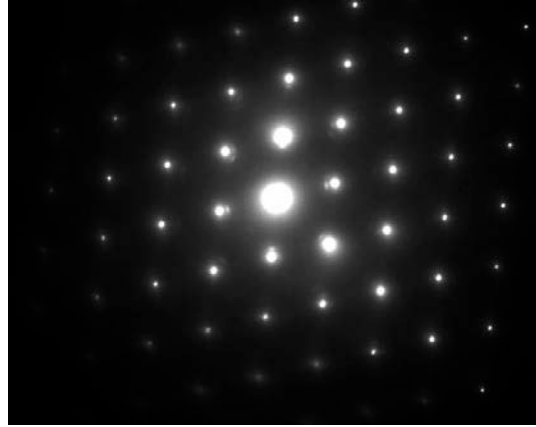


Figure 2.3 [33]

As previously stated, the de Broglie wavelength of high energy electrons is a few thousandths of a nanometer. In contrast, the spacing between atoms in a crystalline solid is a few hundred times larger. Thus, some electrons in the beam will be diffracted by the atoms in the sample. The diffracted electrons originating from the same point in the sample are focused into a beam by the objective lens. This beam is then represented as a spot on the back focal plane (reciprocal space) of the objective lens. The arrangement of spots produced by the diffracted beams is projected onto the image screen and represents the diffraction pattern for the selected area of the material [3-4]. A BF image and corresponding TEM diffraction pattern for a selected area of the Cu-6 wt. % Al alloy disk is shown in Figure 2.4.



Bright Field TEM at 110k X



Diffraction Pattern for [110] Zone Axis

Figure 2.4

In the BF image in Figure 2.4, the dark spheres in contrast with the bright background are the surface contamination particles on the surface of the Cu-6 wt. % Al alloy. Additionally, the diffraction pattern of the same area shows evidence that these contamination particles are distributed epitaxially on the surface of the Cu matrix. The large spots in the diffraction image represent the diffracted beams originating from the Cu matrix. However, smaller spots can be seen in the same locations as the large diffraction spots. These smaller spots originate from the electrons scattered by the surface contamination particles, and since they are in the same location as the diffraction spots produced by the Cu matrix, they are most likely growing epitaxially on the matrix [3-4]. A discussion of the possible mechanisms causing this phenomenon is presented in subsequent sections of this thesis paper.

2.2 TEM Sample Preparation Techniques

As stated in the previous chapter, TEM sample preparation is often a difficult and time-consuming process involving several different steps. All TEM samples must possess two key characteristics. First, the material must be mechanically tough in order to withstand the sample

preparation process. Second, the prepared samples must be electron transparent. For metals and alloys, the final thickness for the area of interest must be about 30-50 nm [1-2,3,5].

Before the final thinning technique is applied, samples must go through a pre-thinning process which involves many steps. Generally, for metals and alloys, the first step in the pre-thinning process is to make thin slices, approximately 250 μm thick, from a bulk sample using a low-speed diamond saw. Next, small disks, commonly 3mm in diameter, are cut from the thin slices using a disk punch or disk cutter. And lastly, the cut disks are mechanically polished to achieve a thickness of approximately 100-120 μm . The grinding material used will depend on the hardness of the sample material. One common grinding material used for the mechanical polishing step is silicon carbide paper, which is available in varying degrees of coarseness. For a hard material, paper with a high level of coarseness can first be used for grinding the sample, followed by a paper with less coarseness to complete the polishing. On the other hand, for a softer material, paper with a medium level of coarseness should be used for initially grinding the sample [1-2,3,5]. Images of a sample at each step of the pre-thinning process is shown in Figure 2.5.

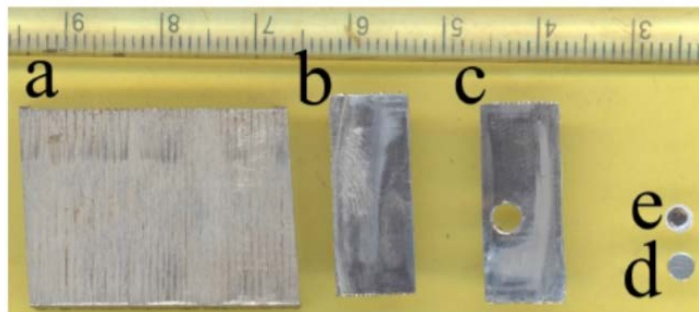


Figure 2.5 [2]

The technique chosen for the final thinning will depend on the type of material being studied and the goals of the TEM analysis. For example, metals and alloys can be prepared using an electropolishing technique, such as jet-polishing. Alternatively, ion beam milling is usually chosen for the final thinning of multi-layer and thin film materials, which can be composed of a combination of semiconductor, metallic, or non-metallic materials. One drawback to both jet-polishing and ion beam milling is that these techniques are unable to create an electron transparent region at a precise location on the sample. However, one TEM specimen preparation technique, focused ion beam SEM (FIB-SEM), can create a specific site of electron transparency with the simultaneous use of SEM and a Ga ion beam. Since the jet-polishing technique was used to prepare the Cu-6 wt. % Al TEM disks, the details of this technique are discussed in the following section [2-3,5].

2.2.1 Jet-Polishing Technique

Jet-polishing is a technique in which conductive samples can be electrochemically thinned for use in TEM. In the jet-polishing set-up, the sample, which acts as a positively charged anode, is placed on a sample holder between two jet nozzles, which act as negatively charged cathodes. Both the sample and the jets are immersed in an electrolyte, and a voltage bias is applied between the jets (cathodes) and the sample (anode). A pump then pushes electrolyte to the jet nozzles, which spray the sample with electrolyte. Once the electrolyte has perforated the sample, a light source on one side of the sample will shine through the perforated area and be detected by a light sensor on the other side of the sample. The area around the perforated area is then considered to be electron transparent. Once the perforation has been made, the applied voltage is turned off and the sample is removed and rinsed in methanol or water to remove any remaining electrolyte. Depending on the material, the rate of thinning in jet-polishing is in the

range of 5-50 $\mu\text{m}/\text{minute}$ [2-3, 5]. Shown in Figure 2.6 is a schematic of a typical jet-polishing set-up.

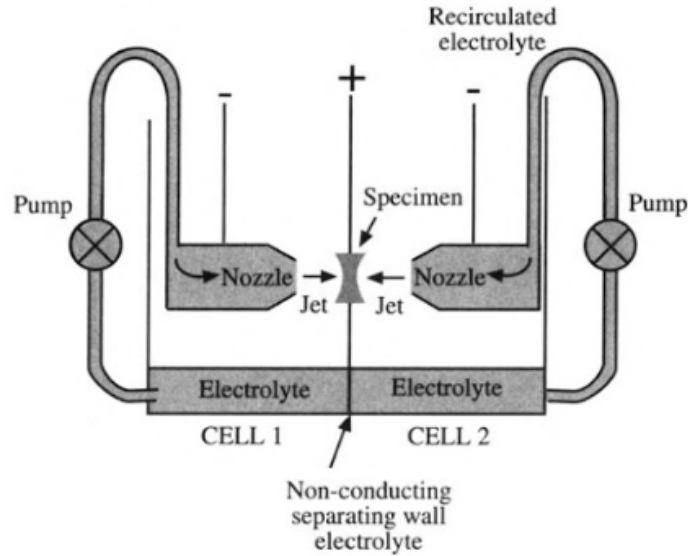


Figure 2.6 [3]

Since it is believed that the surface contamination on the Cu-6 wt.% Al TEM disks originates from the jet-polishing process, a background and discussion on the mechanisms governing electrolytic polishing and thinning will be given in this section. Since its development around a century ago, electropolishing is a technique that has been used to create flat, contamination free, and corrosion resistant surfaces on materials for use in a wide variety of applications. There are two different processes that can occur during electropolishing: macro-electropolishing and micro-electropolishing. Macro-electropolishing refers to a “smoothing” process in which large surface irregularities are removed whereas micro-electropolishing refers to a “brightening” process in which small irregularities less than 1 μm are removed from the surface of a material. Micro-polishing is the process occurring during the thinning of TEM

samples during jet-polishing since large surface irregularities have already been removed during the pre-thinning process [6-7].

The success of jet-polishing in creating quality samples for use in TEM is dependent on several operational parameters, including the electrolyte and the temperature of the electrolyte chosen for the experiment. Usually, the electrolyte must be held at a low temperature, as many of the typical electrolytes used in jet-polishing carry a risk of explosion when exposed to high temperatures. Additionally, the electrolyte should be carefully chosen to make sure it is suitable for the material that is subject to electropolishing. Generally, though, the electrolyte must have certain basic qualities, such as containing complex anions with a large radii and small charge and the ability to form a viscous layer at the metal anode/electrolyte interface. Information regarding suitable electrolytes for different materials can be found in specialized TEM sample preparation handbooks and resources [5,8].

Successful creation of quality TEM samples via electropolishing or jet-polishing is also dependent on choosing an appropriate voltage such that the sample undergoes polishing rather than experiencing etching or pitting. Between a certain range of applied voltages, there exists a current plateau that results in anodic dissolution of metal atoms at the surface of the material through an oxide layer. This effect is shown in Figure 2.7. In the I-V anodic polarization curve, area 1 represents etching at low voltages, area 2 represents polishing, and area 3 represents pitting at high voltages [2, 3-7].

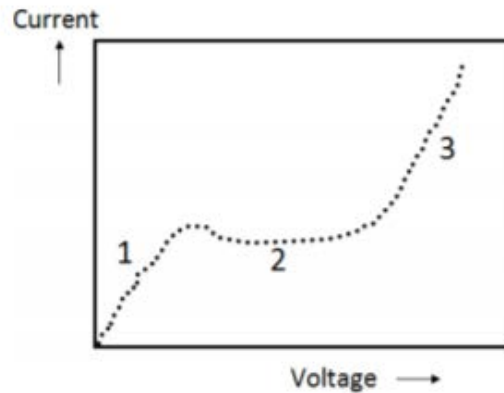


Figure 2.7 [2]

For polishing to occur, a viscous layer must form between the surface of the sample and the electrolyte. When anions in the solution lose hydration water near the anode and are absorbed at the interface of the metal and electrolyte, the viscous layer is formed. Additionally, a thin oxide film must form between surface of the sample and the viscous layer [3, 5-7] A schematic showing these layers in the jet-polishing process is shown in Figure 2.8.

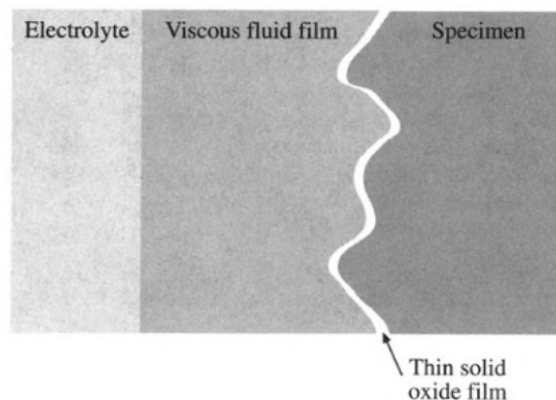
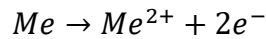


Figure 2.8 [3]

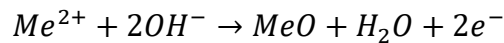
Several theories exist concerning the specific mechanisms that occur during electropolishing, and there is no unification of these theories to date. However, it is generally

accepted that the polishing of the sample surface, rather than etching or pitting, is achieved by selecting a voltage such that a passive oxide film forms upon application of the potential to the anode. The polishing or thinning of the sample surface occurs when metal ions enter the oxide layer through vacant sites in the lattice. The surface of the oxide layer is dissolved by the viscous electrolyte layer when it interacts with anions and forms salts or oxysalts. So long as the applied voltage is kept in the passive range, this process will continue until the desired range of polishing or thinning is achieved. However, if the applied voltage is lower than required for passivity, the thin oxide layer does not form, and the metal is subject to direct dissolution, or etching, by the electrolyte. Alternatively, if the applied voltage is higher than the range of voltages required for passivity, oxygen formation and pitting may occur. The equations for the chemical processes occurring at different regions of the I-V curve can be seen below [3, 5-8].

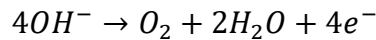
Area I: Direct oxidation of metal atoms in the sample due to etching:



Area II: Formation of an oxide layer that regulates anodic dissolution:



Area III: Formation of oxygen



The generally accepted solid film theory describes the polishing or thinning of the sample as an interaction between the viscous layer and the thin oxide layer. The theory assumes that the viscous layer forms a straight boundary with the bulk electrolyte, meaning that the viscous layer is thinner over high regions of the sample surface and thicker over low regions on the sample

surface. Because of this difference in thickness of the viscous layer over different areas of the sample, high areas of the sample experience a higher local current density and faster dissolution of the sample surface while smaller local current densities on low areas of the sample cause slower dissolution of the sample surface to occur. As polishing continues, roughness of the sample surface will be reduced and eventually become flat [5, 7]. A diagram showing this effect can be seen in Figure 2.9.

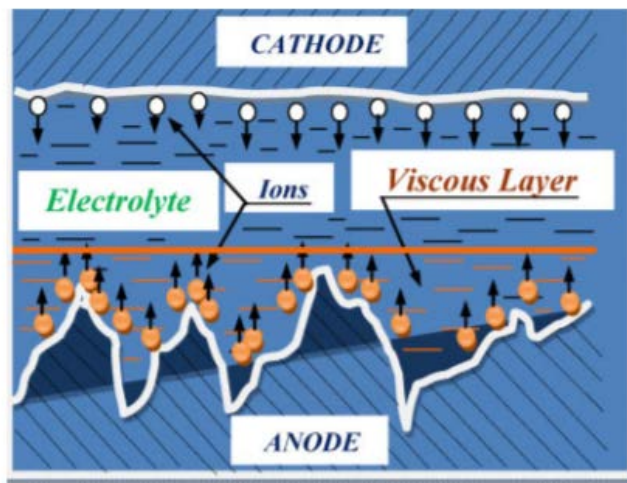


Figure 2.9 [7]

2.2.2 Artifacts Introduced During Jet-Polishing

An artifact can be defined as any change in sample surface features or surface chemistry resulting from the jet-polishing process. Artifacts produced by jet-polishing can be attributed to a few different mechanisms: preferential polishing, redeposition, etching, and pitting. Artifacts due to preferential polishing and redeposition can be attributed to the characteristics of the material, improper choice in electrolyte, or less than optimal polishing conditions, while etching and pitting are controlled by the operational parameters, such as applied voltage, chosen for the jet-polishing experiment [2-3, 5-6].

Preferential polishing occurs in multiphase materials when one phase or element in a material has a different oxidation rate than the other phase or element. If one phase/element in a multiphase material undergoes faster oxidation than the other phase/element, that phase/element will experience anodic dissolution faster than the other phase/element. Alternatively, preferential polishing can cause the phase/element having a slower oxidation rate to accumulate in the layer below the thin oxide layer. Careful selection of an electrolyte suitable to all phases present in the material can solve the issue of preferential polishing. Another issue that can occur in multiphase materials due to preferential polishing is that precipitates can be removed from the surface of the material during the jet-polishing process. However, ion milling for a short time can be used to smooth the edges of the perforation so that the sample is uniformly thinned and representative of the bulk specimen in the electron transparent region [2, 5-6].

Redeposition is another mechanism occurring during jet-polishing that can result in artifacts on the sample surface. During redeposition, dissolution products, such as oxides or sulfur, return to the surface of the material. It also could be possible that these dissolution products never leave the sample surface. This effect can be caused by improper selection of the electrolyte or less than optimal polishing conditions. A study by Rao et. al notes the presence of small contamination particles on the surface of a Ni-Fe-Al ribbon after jet-polishing. A TEM image from this study is compared with an HR-SEM image of the surface contamination particles present on the Cu-6 wt. % Al disks in Figure 2.10. A few sources claim that ion milling for a short time, around 5-10 minutes, will remove the contamination particles [2,5,9].

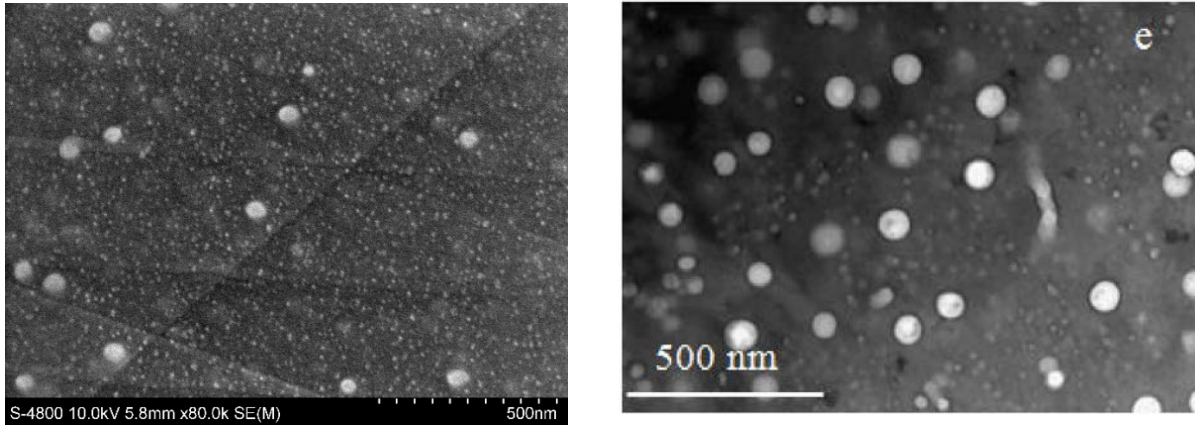


Figure 2.10 [2]

Etching and pitting are caused by incorrect selection of applied voltage, which leads to a current outside of the passive region. If the applied voltage is too low, the oxide layer that regulates the polishing of the sample will not form and the sample will be subject to direct dissolution from the electrolyte. From this effect, the sample can experience localized etching of high density crystallographic planes. Conversely, if the applied voltage is too high, the formation of oxygen can occur, leading to pitting of the sample. This effect can be seen in the form of small holes on the surface of the sample [2,5].

2.3 Mechanisms Responsible for Surface Contamination on Cu-Al TEM Disks

As detailed in the previous sections, the success of the jet-polishing process in producing artifact-free, quality TEM samples is largely determined by finding the optimal operating parameters for a specific material. One source notes that, in the beginning stages of learning, the jet-polishing process is more of an “art” than a science, as so frequently the optimal operating parameters must be determined experimentally through trial-and error for any given material. For the most commonly studied alloys, guidelines are available detailing specific jet-polishing operating parameters, such as a recipe for the electrolyte and a recommendation for the

electrolyte temperature, applied voltage and current, along with notes about any artifacts that can result from the polishing, such as the presence of an oxide film. However, for many alloys, such as the Cu- 6 wt. % Al alloy, only a basic recommendation for the composition and temperature of the electrolyte is available, and sometimes even this information varies by source. Thus, without prior knowledge of the optimal operating parameters for a specific material or alloy, it is very easy to mistakenly choose operating parameters, such as the electrolyte, that produce less than optimal polishing conditions, leading to artifacts on the sample surface after the polishing is performed. In the jet-polishing experiments done with the Cu- 6 wt. % Al TEM disks, the electrolyte used was roughly 2/3 methanol and 1/3 nitric acid. While this electrolyte composition is in accordance with the recommendations for “Cu” or “Cu and its alloys” in various sources, these same sources also list alternative acceptable electrolyte recipes for “Cu and its alloys”, such as 25% phosphoric acid and 25% ethanol in water. Thus, it can be confusing to select a suitable electrolyte for alloys that are not specifically mentioned in sources. Because the literature notes that artifacts, such as oxides, can occur when the composition of the chosen electrolyte is not optimal, it is possible that the surface contamination on the Cu- 6 wt. % Al TEM disks is due to this effect [3,5,10].

Another possible mechanism that could be causing the surface contamination issues on the jet-polished Cu- 6 wt.% Al TEM disks is preferential polishing. As can be seen below, Al is much less noble than Cu, meaning that it is more easily oxidized than Cu when measured against the standard hydrogen potential.

Oxidation Reaction	Volts vs. SHE
$Cu \rightarrow Cu^{2+} + 2e^{-}$	-.34
$Al \rightarrow Al^{3+} + 3e^{-}$	1.66

Due to preferential polishing, it is possible that the Al atoms in the Cu- 6 wt. % Al TEM disks are oxidized more quickly and enter the oxide layer, forming aluminum oxide molecules, faster than the Cu atoms. This effect would then imply that the oxide layer contains a larger percentage of Al than is characteristic of the composition of the bulk alloy. When the polishing is completed, and the applied voltage is stopped, it could be possible that the aluminum or aluminum oxide remaining in the oxide layer settles on the sample surface as products of the polishing process [2,5,11].

2.3.1 Evidence in Literature

The problem of surface contamination occurring during jet-polishing has been reported in scientific literature for the past several decades. Many of these studies mention that surface contamination on TEM disks prepared using jet-polishing was discovered when compositional analysis, either EDS, XPS, or Auger electron spectroscopy, was performed on the TEM disks. These studies report surface contamination in the form of either a thin film, spherical particles, or both [9,12]. This section will examine these studies and compare relevant findings with the results of this research.

The three studies discussed here were chosen because the TEM samples in question were composed of binary alloys containing Cu and Al. In these studies, compositional analysis was carried out using X-ray photoelectron spectroscopy (XPS) and found that solute to solvent characteristic intensity ratios varied with depth from the sample surface after electropolishing.

For example, one study by Thompson et al. found that the Cu/Al intensity ratio was very high at the surface of electropolished Al based-Cu alloy TEM disks and approached alloy composition levels with increasing depth into the disk. The study reports that this effect is due to the deposition of a thin layer of Cu on the sample surface during electropolishing and that ion cleaning did not remove the Cu-rich film on the surface of the sample [9,12]. Morris et al. reached a similar conclusion while studying Al-4% Cu alloy disks. In this study, TEM disks were created using jet-polishing followed by ion milling to remove any debris from the jet-polishing process. The samples were evaluated using TEM with EDS attachment and also XPS. During XPS analysis, an intensity spectrum was obtained to determine the Cu/Al intensity ratio at the sample surface. Ion etching was used to remove layers of the disk, and an intensity spectrum was recorded at each layer. The XPS analysis revealed that the jet-polished Al- 4% Cu disks had large Cu/Al intensity ratios at the sample surface, with the ratios exponentially decreasing as depth into the sample was increased. Morris et. al also performed XPS analysis on electropolished Al-based Zn alloys and Al-based Ag alloys and discovered the existence of an Ag-rich surface film in the Al-Ag alloys but did not find evidence of a surface film in the Al-Zn alloys. Additionally, the study by Morris et. al revealed Cu-rich particles present on the surface film upon SEM imaging. The SEM image from this study is compared with an HR-SEM image of the surface contamination particles present on the Cu- 6% Al disks in Figure 2.11. In its conclusion, the Morris et. al study determined that traditional ion cleaning was successful in removing the surface particles. Regarding the surface film, the study claims that only ESCA ion cleaning can be used to remove the Cu-rich surface film [9]. A third study, by Pountney and Loretto, reports a thin film on the TEM sample surface of an electropolished Cu-Al alloy. The effect was discovered when Auger electron spectroscopy was performed on the TEM samples.

The study notes that the deposited solute-based film on the sample surfaces was absent on samples that were hand polished [12].

The preferential polishing discussed in the previous section could be used to explain the existence of the thin solute-based films observed in these studies. In all of the studies summarized above, with the exception of the Pountney and Loretto experiments, which studied a Cu-based Al alloy, it is reported that the thin films on the surface of the TEM disks are composed of the more noble element in the binary alloy being studied. For example, it is the Cu in the Al-based Cu alloy and the Ag in the Al-based Ag alloy that are forming the surface films. As discussed in the previous section, sometimes the element that is less easily oxidized forms a layer below the oxide layer during the jet-polishing process. It is possible that, after jet-polishing was performed, the films of the more noble elements of the binary alloys remained on the surface of the TEM disks investigated in these studies. Further adding to this idea is the fact that a thin film of Zn was not detected on the Al-based Zn alloy studied by Morris. et. al., suggesting that because Zn is less noble than Al, it was more easily oxidized and did not form a layer under the oxide layer during the jet-polishing process [2,5,6,11].

While these studies are beneficial in that they confirm that surface contamination occurs during electropolishing (or jet-polishing) in binary alloys containing Cu and Al, they do not suggest a mechanism as to the reason why the contamination exists on the surface of the TEM disks after the electropolishing process. Additionally, Morris et. al, the study which confirmed the existence of Cu-based solute particles through SEM images, does not report whether the particles are epitaxially aligned with the alloy matrix [9]. The next section aims to provide possible explanations to these observed phenomena.

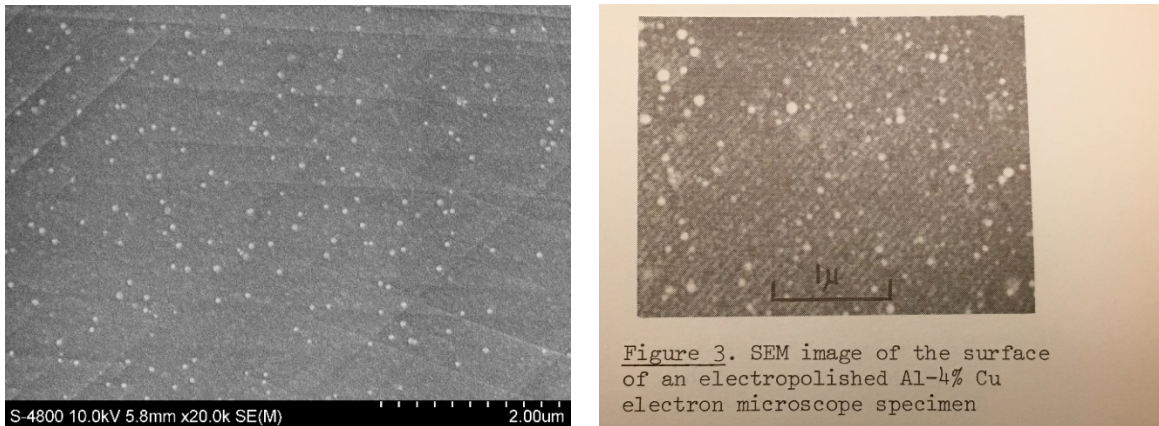


Figure 2.11[9]

2.3.2 Mechanisms Describing Epitaxial Particle Growth

As discussed previously in the TEM background section, the contamination particles on the surface of the Cu- 6 wt. % Al alloy disks appear to be growing epitaxially on the Cu matrix. Epitaxy is defined as the growth of a crystalline film on a crystalline substrate in a manner such that the atomic arrangement of the film aligns with the crystal structure of the substrate, and a coherent interface between the film and the substrate is formed. Epitaxy is an important tool in producing thin films in semiconductor, electronic, and optical applications, and there are several techniques used for depositing thin films on a substrate, including vapor-phase, liquid-phase, and molecular beam epitaxy. However, contamination on the Cu-6 wt. % Al alloy disks is deposited on the surface of the disks through a mechanism occurring during the jet-polishing process. Since epitaxy generally refers to the growth of a surface film, the question is raised as to how the material deposited onto the surface of the Cu-6 wt. % Al alloy disks is growing epitaxially in the form of small particles. Epitaxial growth is a complex process, largely influenced by the method used to deposit atoms on the substrate, the type of materials composing the film and the substrate, and the conditions under which growth occurs, so only a brief overview of the

fundamental stages of the process and a discussion of various thermodynamic and kinetic epitaxial growth modes will be given in this section [14-16].

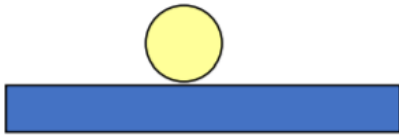
The first step in the epitaxial growth of a thin film is the deposition of atoms on the surface of the substrate material. As mentioned previously, there are several methods used to deposit atoms on the substrate material, and the method chosen will depend of the goals of the epitaxial growth and the type of materials used for the substrate and the thin film. Once deposited on the substrate, atoms weakly bond with the surface atoms of the material and diffuse across the surface to low-energy locations, which are also referred to as epitaxial sites. The atoms then attach to other atoms at the epitaxial site in a process known as nucleation. As more atoms arrive on the surface of the material, they join clusters of atoms at the nucleation sites, leading to epitaxial growth. There are several modes of growth that can occur during epitaxy, and they are generally either driven by thermodynamic processes or kinetic processes. These growth modes are discussed in the remainder of this section [14-16].

Three growth modes, in regard to thermodynamics, can be used to describe the different ways in which material can grow epitaxially on the surface of a substrate: the Frank-van der Merwe (FM) mode, the Volmer-Weber (VW) mode, and the Stranski-Krastanov (SK) mode. In all three growth modes, atoms arriving on the substrate diffuse across the surface and nucleate in a manner that reduces the total energy of the film/interface/substrate system. In the Frank-van der Merwe (FM) mode, atoms arriving on the substrate grow layer-by-layer because the sum of the interface energy and the film surface energy is lower than the substrate surface energy. Conversely, in Volmer-Weber (VW) mode, the sum of the interface energy and the film surface energy is greater than the substrate surface energy, and thus it is energetically favorable for atoms grow epitaxially in the form of small islands. Lastly, in Stranski-Krastanov (SK) mode, a

hybrid of FM and VW modes, it is at first energetically favorable for atoms arriving on the substrate grow as a film and then as islands once the film has formed [14-16]. A diagram of the three thermodynamic growth methods and their associated energy conditions is show in Figure 2.12.

VM Growth Mode:

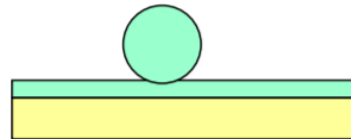
$$\gamma_{sub} < \gamma_{film} + \gamma_{interface}$$



SK Growth Mode:

$$1^{st}: \gamma_{sub} \geq \gamma_{film} + \gamma_{interface}$$

$$2^{nd}: \gamma_{sub} < \gamma_{film} + \gamma_{interface}$$



FM Growth Mode:

$$\gamma_{sub} \geq \gamma_{film} + \gamma_{interface}$$



Figure 2.12 [13]

Upon initial consideration, it seems that the epitaxial growth of the contamination particles on the surface of the Cu-6 wt. % Al alloy disks could be attributed to either the Volmer-Weber (VW) or Stranski-Krastanov (SK) modes of growth. However, the issue with using these modes to describe the epitaxial growth of the surface contamination particles is that these thermodynamically-driven processes occur near equilibrium conditions, in which the epitaxial

growth mode and surface morphology is always a result of the atoms diffusing across the surface of the material and growing in the lowest possible free energy configuration, regardless of the path taken by the atoms across the surface of the material to achieve these conditions [15-16]. While the equilibrium surface diffusion and epitaxial growth usually occurs at high temperatures, redeposition material on the surface of the Cu-6 wt. % Al alloy disks grows epitaxially at a relatively low temperature. Typically, the electrolyte used during jet-polishing is usually held at room temperature or lower [2,5]. Several papers in scientific literature report that surface diffusion and epitaxial growth of metallic thin films and particles on a metallic substrate are possible at room temperature and below but note that these processes are driven by kinetics rather than thermodynamics [15-19].

Away from equilibrium conditions, at low temperatures, atoms encounter energy barriers upon moving across the surface of the substrate. These energy barriers influence diffusion rates and the type of film growth morphology that will occur. Generally, there are three basic kinetically-driven growth modes: step-flow growth mode, layer-by-layer growth mode, and multilayer growth mode [15-16] These three growth modes are represented in Figure 2.13.

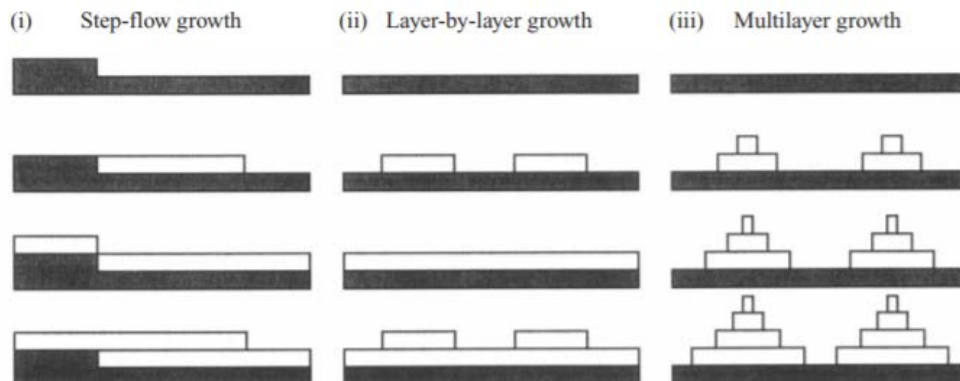


Figure 2.13 [16]

Step-flow growth involves atoms moving across the surface of the substrate and utilizing “steps” as structures upon which to grow epitaxially layers. This concept is represented in 3D Figure 2.14.

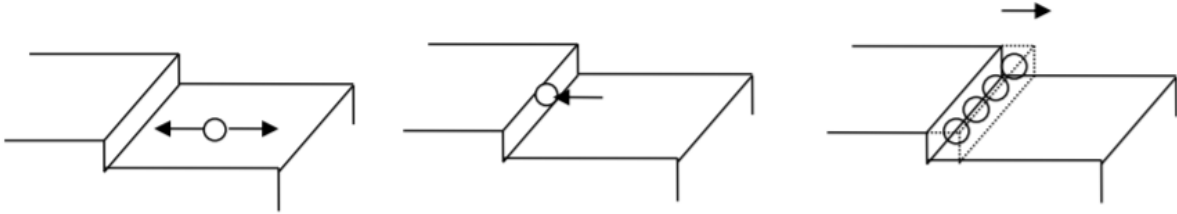


Figure 2.14

[13]

Step-flow growth typically occurs at high temperatures closer to equilibrium conditions due to the energy barriers encountered by the atoms in this growth mode. For example, a hypothetical atom on the terrace above the step seen in Figure 2.14 would require a certain amount of energy to descend the step and attach to it. Conversely, if the atom shown in Figure 2.14 was located at a distance further from the step than is shown in the image, it would also require a large amount of energy to diffuse across the surface and attach to the step. At low temperatures far away from equilibrium conditions, it is unlikely that atoms moving on the substrate would be able to overcome these energy barriers, and thus the step-flow growth mode is not the most probable growth mode at low temperatures. The layer-by-layer and multilayer kinetic growth modes are much more likely at low temperatures. In these growth modes, atoms diffusing on the substrate attach to one another and nucleate islands on flat terraces. This concept is represented in Figure 2.15. While these growth modes do not require the atoms to overcome the energy barriers like those encountered in the step-flow growth mode, both layer-by-layer and multilayer growth

modes suggest that a large flux of atoms on the substrate would need to be present in order for the atoms to easily attach and nucleate islands [14-16].

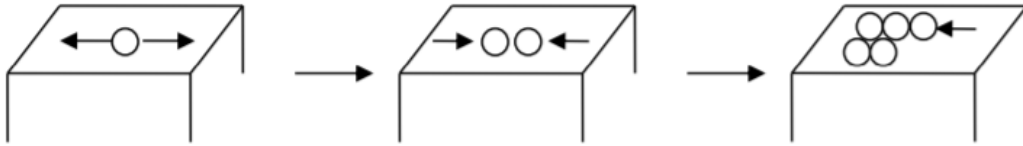


Figure 2.15 [13]

Whether the nucleation and growth of the atoms follows the layer-by-layer growth mode or the multilayer growth mode is dependent on diffusion processes occurring between the layers of growth. In Figure 2.13 (ii), representing layer-by-layer growth, it can be seen that as new islands begin to form on top of full formed layers, a step is created between the island and the layer below. If atoms deposited on the surface of the island can easily overcome the energy barrier to descend the step between the island and the layer below, the islands will eventually coalesce and form a second layer on top of the one below, leading to layer-by-layer growth mode. However, if the atoms on the surface of the island cannot overcome the energy barrier to descend the step, they will attach to other atoms that are subsequently deposited on the surface of the island. These atoms will then nucleate and grow smaller islands on top of the ones below, leading to the multilayer growth mode that can be seen in Figure 2.13 (iii) [14-16].

After reviewing the thermodynamically-driven and kinetically-driven epitaxial growth modes, it seems that the kinetically-driven multilayer epitaxial growth mode could be a possible mechanism for explaining how the surface contamination on the Cu-6 wt. % Al alloy disks is growing epitaxially at room temperature or below. In contrast to the thermodynamically-driven Stranski-Krastanov and Volmer-Weber epitaxial growth modes, in which atoms easily diffuse

across the substrate to nucleate and grow in equilibrium configurations that reduce the surface energy and strain effects between the thin film and the substrate, the diffusion rate and nucleation/growth of islands in the kinetically-driven multilayer growth mode are controlled by energy barriers and atomic interactions, leading to the most stable epitaxial growth configuration that is possible in the low-temperature non-equilibrium conditions. It is possible that during the jet-polishing process, atoms of the dissolution material are arriving on the surface of the Cu-6 wt. % Al alloy disks and diffusing toward low-energy epitaxial sites, and once there, attach to one another and nucleate islands. Since, at the typical temperatures of the electrolyte used in the jet-polishing process, the atoms arriving at the surfaces of islands likely do not have the energy to make the step down to the layer below, they possibly attach with other atoms on the surface of the island and grow in a kinetically-driven 3D epitaxial growth mode. Certainly, this theory deserves further study as epitaxial growth is a complex subject, but the review of epitaxial growth modes presented in this thesis at the least provides evidence that epitaxial growth is indeed possible at low temperatures and also that it does not always occur in the form of a thin film, but can rather take many forms, including the form of small particles [14-19].

CHAPTER II

PART II: SEM AND ION MILLING

2.4 Theoretical Background for Characterization and Experiments

HR-SEM and ion milling were both used extensively for this research and thus a theoretical background for each is given in this section. HR-SEM was chosen for this research over conventional SEM due to the high magnification needed to image the particles. The contamination particles on the surface of the Cu- 6 wt. % Al alloys disks have an average diameter range of between 15-60 nm, and thus require a magnification of 40k-120k X to achieve high resolution imaging. Achieving this magnification with high resolution was only possible using HR-SEM. However, much of the theoretical background and operating parameters pertaining to HR-SEM are similar to conventional SEM, and so a general background for SEM is given, along with a discussion of any differences between SEM and HR-SEM.

2.4.1 Theoretical Principles of HR-SEM

Scanning electron microscopy uses a high energy beam of electrons as a probe to scan the surface of a sample. The electrons scattered by the incident beam can resolve images of the sample surface that show topography and contrast characteristics. It is important to keep in mind that the image produced by the SEM is not actually an optical image of the sample, but rather a representation of the sample surface characteristics created using signals gathered from the scattered electrons. SEM uses an electron gun, a thermionic metal source usually composed of tungsten, to provide a high intensity source of electrons. Electrons are drawn from a heated filament by a low bias voltage between the electron source and a cylindrical cap. The beam is focused by an electrostatic field and accelerated into the chamber through an anode below the

cylindrical cap. The beam then passes through condenser lenses, which focus the electron beam to an area about 0.5-5 nm in diameter. Lastly, the beam is directed through scanning coils in the final lens which direct the beam into x and y axes so that the electron beam scans the sample surface in a raster pattern [1,20-23]. A diagram of a typical SEM is shown in Figure 2.16.

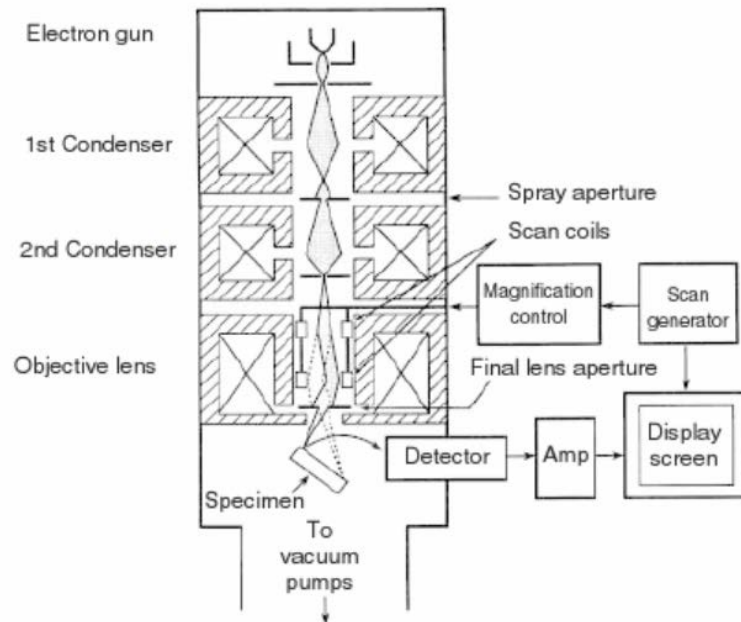


Figure 2.16 [20]

A few different types of electrons can be emitted from the sample in response to the incident beam, and each type provides different information about the sample surface. One type of electrons emitted from the sample is secondary electrons, which are created when the energy of the incident beam knocks out electrons from their positions in the samples and causes them to be ejected from the sample. Back scattered electrons are electrons from the primary beam that have been scattered by the sample surface. These two different types of electron response signals are shown in Figure 2.17 [1, 20-23].

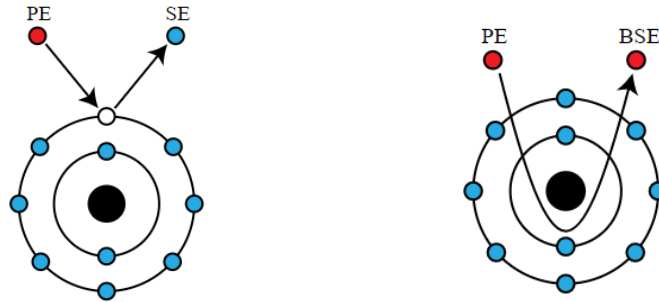


Figure 2.17 [24]

SEM uses two imaging modes, SEI mode and BEI mode. SEI mode creates an image showing the topographic characteristics of the sample surface using secondary electrons. The emitted electrons are collected by a positively biased detector to create an image. SEI mode can create high resolution surface topography images because more electrons will strike high areas of the sample surface than low areas of the sample surface. Since the high areas are more exposed to the incident electron beam, they will produce larger secondary electron intensity than the low areas of the sample. Thus, an image of surface topography can be analyzed using SEI mode. BEI mode, although less commonly used than SEI mode, is useful in determining the surface characteristics of a sample. BEI mode uses back scattered electrons to create an image of the sample surface that can show both topography and contrast. Additionally, BEI is capable of two different imaging modes, compo mode and topo mode. In compo mode, a composition contrast image can be created using backscattered electrons. If a sample contains atoms of two or more different elements, the heavier elements will produce more backscattered electrons, and the detector will record a higher intensity of backscattered electrons from areas of the sample surface containing the heavier element. Thus, the image created using compo mode will show areas of the sample surface containing heavier elements as brighter than the areas of the sample surface containing lighter elements. In topo mode, an image showing the surface topography

characteristics of the sample can be obtained. If the surface of the sample is even, both sides of the detector will record an equal intensity of backscattered electrons. However, if the sample surface is uneven, the two sides of the detector will record uneven backscattered electron intensity. In this way, BEI mode can be used to create a surface topography image using backscattered electrons [1,20-23].

There are several factors which can affect the resolution of SEM images, including acceleration voltage, beam current, working distance, and objective aperture size. A large acceleration voltage of the incident beam of electrons will produce a higher resolution image. While this statement is generally true for conventional SEM, a small acceleration voltage is usually chosen in HR-SEM. At the short working distance and high magnification used in HR-SEM, using a low acceleration voltage is necessary because a high acceleration voltage would create an excess of secondary electrons and produce a noisy image. A larger spot size creates a better contrast, but also poor resolution. The spot size is the electron beam size per pixel. If the spot size is too large in comparison to the pixel size, the image will be blurred. To correct this, the magnification must be reduced to match the spot size. The working distance is the distance between the objective lens and the sample. A short working distance creates a high-resolution image because the field of focus is small. A long working distance will yield a low-resolution image because the field of focus is large. The resolution is inversely proportional to the aperture size. Thus, a large objective aperture will produce low resolution, while a small aperture size will produce high resolution [1,20-23].

2.4.1.1 EDS Analysis

One limitation of SEM is that it cannot determine the composition of a sample. However, certain attachments for SEM can be used to overcome this limitation. EDS, Energy Dispersive

X-ray Spectroscopy, is an SEM attachment that can be used to determine the composition of a sample. When the high energy electron beam in an SEM strikes an atom in the sample, it may displace one of the inner shell electrons in the atom, causing an electron hole. An electron from an outer shell then takes the place of the inner shell electron. This transition creates an X-ray characteristic of both the element and the specific transition between shells [1, 21]. The concept is shown in the Figure 2.18.

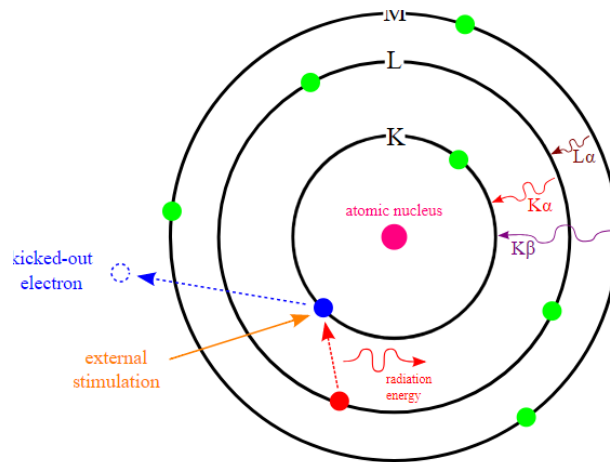


Figure 2.18 [25]

The EDS attachment and associated software is capable of various types of composition analysis. First, EDS can provide an elemental spectrum analysis, in which the intensity of detected X-rays is plotted against the characteristic X-ray energies. EDS spectrum analysis is most commonly used to determine the composition of a specific spot or line on the sample surface. EDS can also be used for elemental mapping of the sample surface. With mapping analysis, an entire area of the sample surface is analyzed to determine what elements are present in that area. The EDS software uses different colors to represent different elements for the selected area [1, 20-23].

2.4.2 Low-Angle Ion Milling

Low-angle ion milling is generally used for the final thinning step in the TEM sample preparation of non-conductive samples. Generally, a high energy Ar ion beam (3-5 keV), having a low angle of incidence ($3-5^\circ$) with respect to sample, bombards the surface of the sample, thus removing material and thinning the sample. A schematic of an ion milling machine is shown in Figure 2.16. If used for the purpose of thinning samples for use in TEM, ion-milling is usually a time-consuming process, as material is sputtered from the surface at a rate of a few μm per hour. However, if the goal of the ion milling is to merely clean contamination from the surface of the sample without thinning it, ion milling can be performed for a shorter time, such as five to ten minutes [2-3,5].

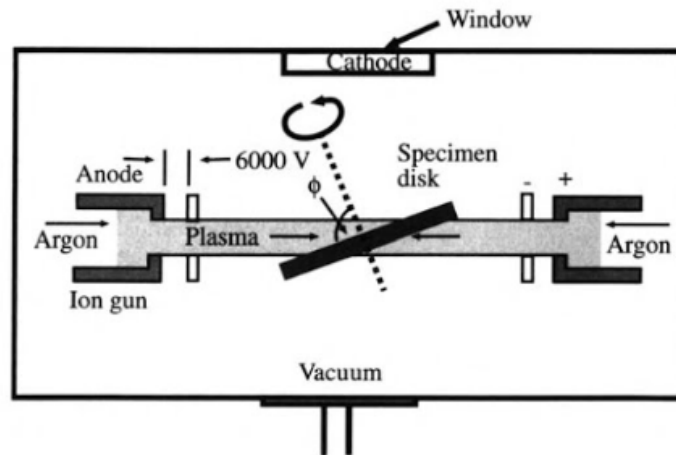


Figure 2.19 [3]

CHAPTER III

EXPERIMENTAL PROCEDURE

The Cu- 6 wt.% Al TEM disks studied in this research were previously created by our group using the methods outlined in Chapter II. Additionally, the alloy was subjected to four different aging times and temperatures before the TEM sample preparation process was carried out. Following is a list of the aging times and temperatures used:

1. 950° C for 1 hour (2 Samples)
2. 250° C for 28 days (2 Samples)
3. As-Quenched (2 Samples)
4. 450°C for 19 hours (1 Sample)

3.1 HR-SEM Characterization

The samples were investigated using the Hitachi S-4800 II HR-SEM in CCMB at UTA. The microscope features a theoretical resolution of 1 nm and can be operated at acceleration voltages ranging from .5 keV to 30 keV.

The original TEM images revealed roughly spherical shaped particles having an average diameter of between 15-60 nm. The first consideration in imaging the surface contamination particles with HR-SEM was choosing the location on the 3mm TEM disks to search for the particles. Because the particles were believed to be caused by redeposition during the jet-polishing process, the logical area to begin searching for the particles was the electron transparent perimeter around the perforation created by the electrolyte jets. As an example, an HR-SEM image of this area on one of the Cu-6 wt.% Al TEM disks shown in Figure 3.1.

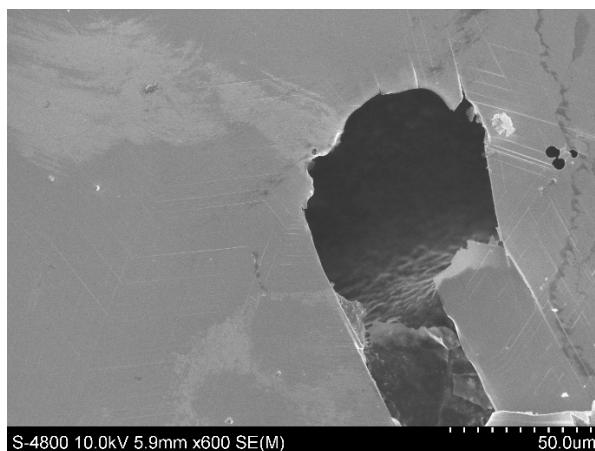


Figure 3.1

Once HR-SEM imaging confirmed the existence of the contamination particles on the surface of the samples, the focus of this portion of the research turned to selecting operating parameters, such as magnification, working distance, and acceleration voltage, which would produce optimal images in terms of resolution and contrast. The contamination particles were visible beginning at a magnification of around 20k-40k X, and images were taken starting in this magnification range and up to around 120k X. Around 40k-80k X proved to be the optimal magnification for imaging the particles because this magnification range provided sufficient detail of the individual particles while also lending an overall image of the particles as a group and their distribution on the sample surface. To obtain a small field of view, a working distance of 5 mm was chosen. Working distances larger than 10 mm were only useful in imaging the particles up to around 60k X, after which quality resolution of the particles began to decline. An acceleration voltage of 10 kV proved to be best in providing both high resolution and adequate brightness for imaging the particles. Acceleration voltages lower than 10 kV did not provide enough brightness for imaging the particles, while those larger than 10 kV created excessive noise in the images. Additionally, a beam current of 15 μ A was used for imaging all the samples.

After these optimal operating conditions were determined, several images of the surface contamination particles were taken for each of the seven samples and were compared with the original TEM images of the same samples [1,20-23].

3.1.1 EDS Analysis and Limitations

Compositional analysis for the contamination particles was attempted with the EDS attachment on the Hitachi S-4800 II HR-SEM. However, there were a few complicating factors that prevented the EDS analysis from being useful in producing data from which accurate quantitative elemental information about the sample could be determined. First, to perform EDS analysis, a working distance of 15 mm is required. Usually, EDS analysis, either composition spectrum analysis or elemental mapping, is performed at magnifications between 10k X and 40k X. However, obtaining high resolution images of the small particles at the relatively large working distance of 15 mm and low magnification proved difficult. Additionally, the nanometer thickness scale of the samples caused issues with generating strong characteristic X-ray signals. Generally, characteristic X-rays are generated at depths of 1-3 μm below the surface of the sample, and thus the Cu-6 wt.% Al TEM disks, having a diameter of approximately 30-50 nm in the area of interest, were too thin for generating the strong X-ray signals necessary for accurate quantitative EDS analysis [23]. This concept is illustrated in Figure 3.2. Future experiments focusing on TEM sample surface contamination might consider the use of XPS or Auger electron spectroscopy for studying surface contamination composition on TEM disks, as both methods are suited for composition analysis of thin specimens and surfaces [9,12]. Despite these limitations, the results of the EDS analysis are presented in the following chapter to give a general idea about the elements present and the relative amounts of each in the Cu-6 wt.% Al TEM disks.

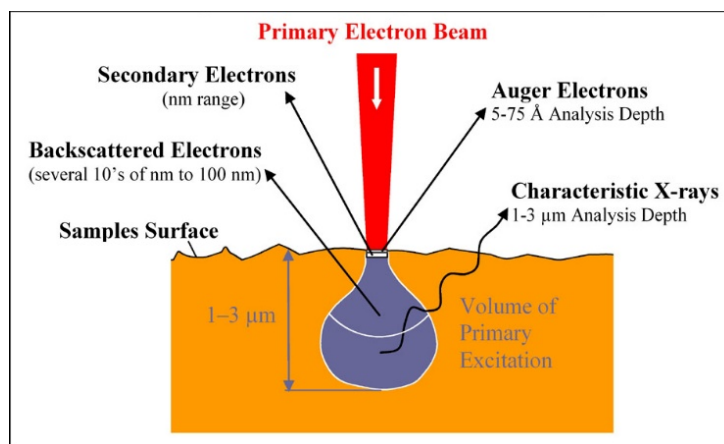


Figure 3.2 [26]

3.2 Low-Angle Ion Cleaning

After obtaining quality HR-SEM images of the surface contamination particles, low-angle ion cleaning was done with all seven samples in an attempt to remove the particles from the surface of the samples. The ion cleaning was performed using a Gatan Model 691 precise ion polishing systems (PIPS). Several operational settings were carefully chosen before conducting the ion cleaning. First, a cleaning time of 5 minutes was chosen to ensure that the samples did not experience any thinning. Additionally, the angle of the ion guns was set at 4° incident to the sample surface and the energy of the ions guns was set at 4 keV.

3.3 HR-SEM Post-Ion-Cleaning

After the Cu-6 wt.% Al TEM disks were ion cleaned, they were investigated again using HR-SEM to determine if the surface contamination particles were removed by the ion cleaning. Care was taken to observe several areas on each of the ion-cleaned samples to ensure that any remaining surface contamination was identified and imaged. Also, exhaustive image analysis was done in comparing the pre-ion cleaning images and post-ion cleaning images of each sample

to identify any differences in the shape or size of the contamination particles before and after ion cleaning was done. The results of these experiments are presented in Chapter IV.

CHAPTER IV

RESULTS

As stated in previous chapters, the first goal of this thesis research was to further examine the surface contamination particles previously seen on TEM images of the Cu-6 wt. % alloy disks using HR-SEM. The next step was to compare the HR-SEM and TEM images of the surface contamination particles, and to note any differences or similarities between the images. Lastly, low-angle ion-cleaning was performed on all the samples in an attempt to remove the surface contamination particles, and HR-SEM was again utilized to determine if the ion cleaning technique was successful in removing the particles. The results of these experiments are detailed in this chapter.

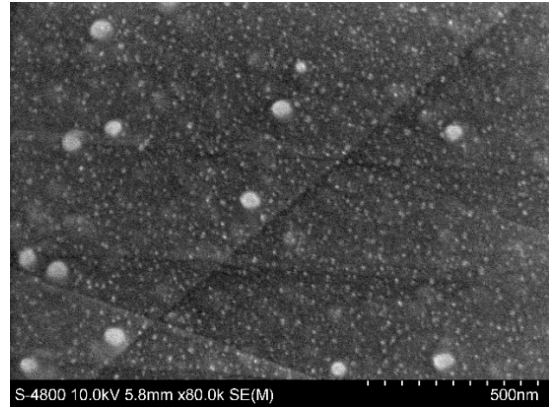
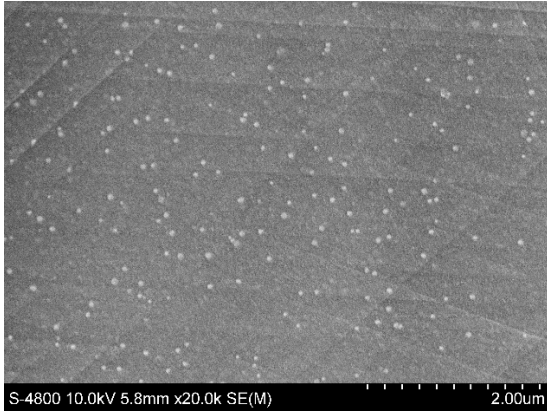
4.1 HR-SEM Characterization of Surface Contamination Particles

The aim of this portion of the experiment was to use HR-SEM to identify and characterize, in terms of size, shape, and distribution, the contamination particles on the surface of Cu-6 wt.% alloy disks. HR-SEM images were taken at various points around the electron transparent perimeter of the perforation created by the jet-polishing process. Several images of each sample were taken at varying magnifications, and a high magnification and low magnification HR-SEM image for each sample can be seen in Figure 4.1.

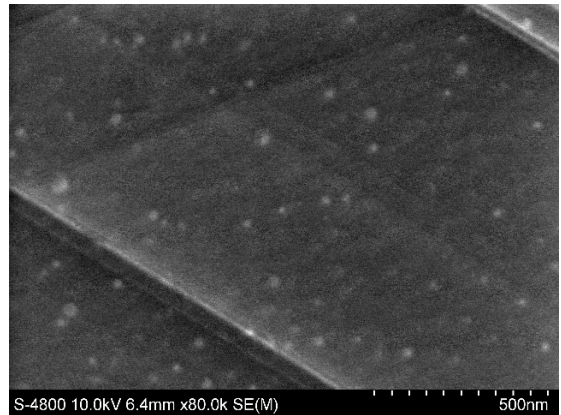
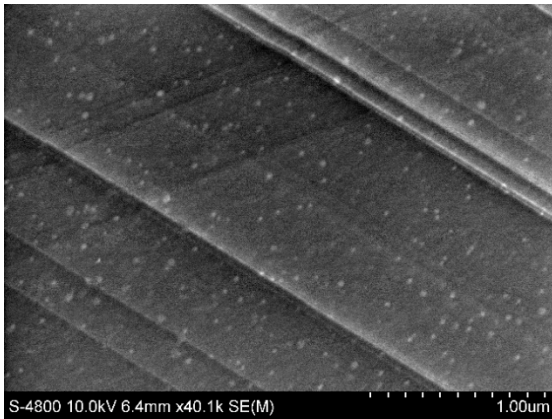
4.1.1 Variance in Shape and Size of the Surface Contamination Particles

Upon observation of the HR-SEM images of the surface contamination particles, it is evident that the shape and size of the particles varies among different samples. For example, very large particles, around 250 nm in diameter, having an almost triangular shape are seen in Figure 4.1 e), while smaller particles, around 5-10 nm in diameter, are seen in Figure 4.1 c) and d).

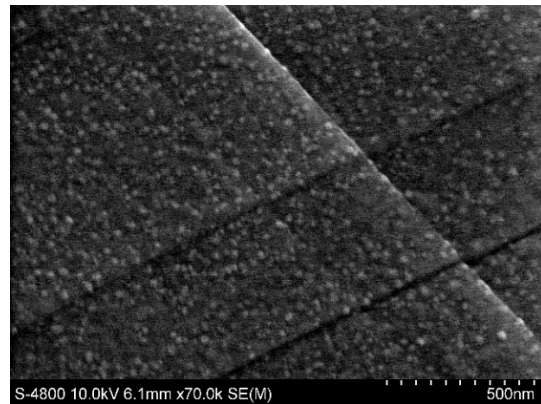
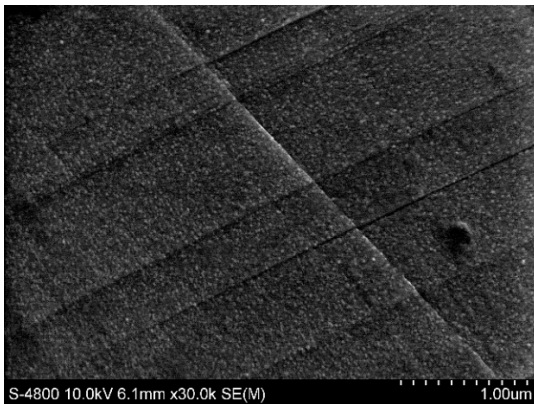
a) As-Quenched: Sample 1



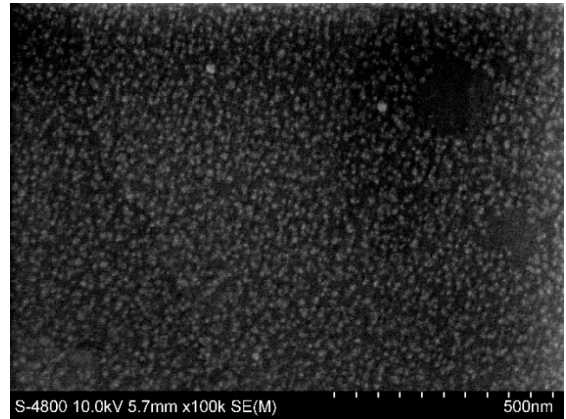
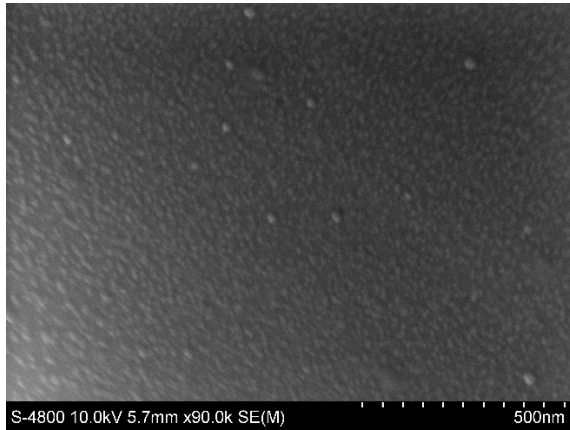
b) As-Quenched: Sample 2



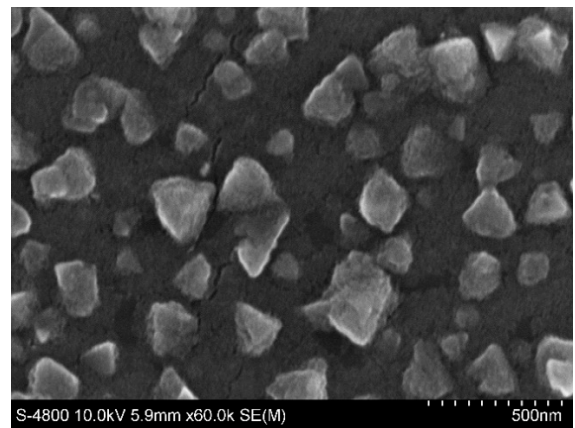
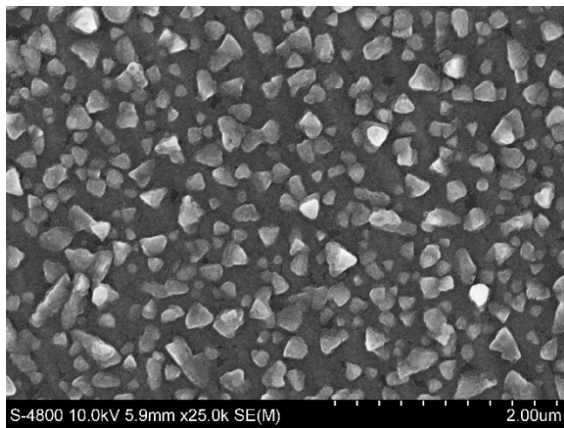
c) Aged at 950° C for 1 Hour: Sample 1



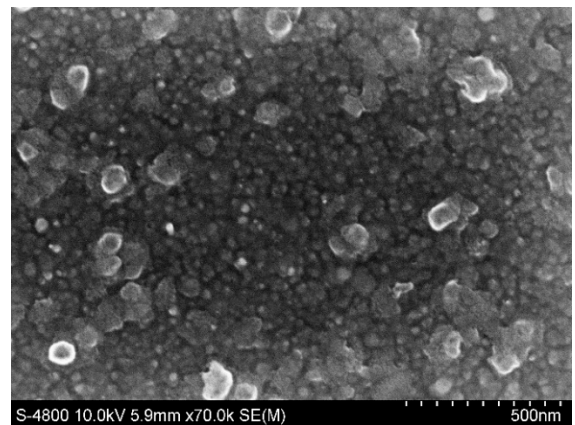
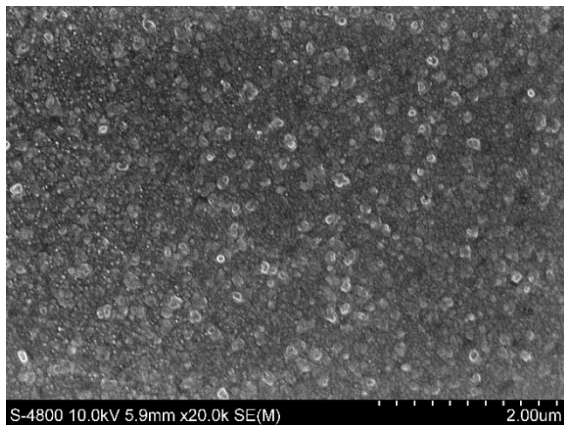
d) Aged at 950°C for 1 Hour: Sample 2



e) Aged at 250°C for 28 Days: Sample 1



f) Aged at 250°C for 28 Days: Sample 2



g) Aged at 450°C for 19 Hours: Sample 1

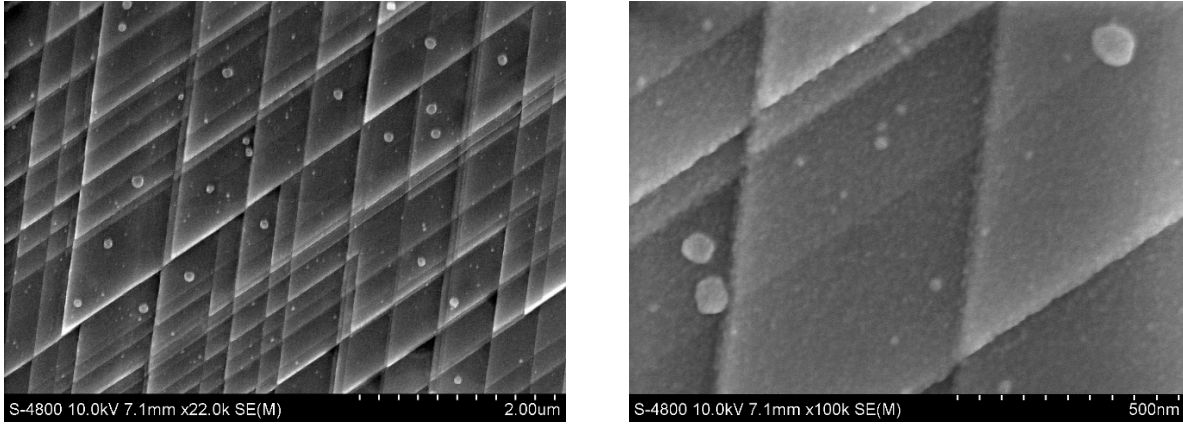


Figure 4.1

One possible explanation for this phenomenon comes from a study by Leonard et. al [27], which observed the formation of InAs islands on GaAs via the Stranski Krastanov (SK) epitaxial growth mode. The study used atomic force microscopy (AFM) to image the InAs SK islands and found that the most uniform islands, in terms of shape and size, were found in the initial stages of island development. The AFM images from this study can be seen in Figure 4.2. It can be seen that the SK islands in the first three images (top row) of Figure 4.2, which show the initial stages of island development, are the most uniform in shape and size. Then, in the last three images (bottom row), showing the continued stages of development, the islands begin to become less uniform [27]. While it is unlikely that the surface contamination particles on the Cu-6 wt. % alloy disks are growing epitaxially on the Cu matrix via the Stranski-Krastanov or Volmer-Weber growth modes due to the high temperature required for these growth modes to occur [14-16], the concept that the size and shape of epitaxially grown islands can change over time could be applied to this research to explain the variance of shape and size among the surface contamination particles seen among the samples in Figure 4.1. For instance, if two of the TEM

samples were prepared at the same time using jet-polishing, but only one of the samples was viewed in TEM shortly after, then the sample viewed in TEM first might have smaller, more uniform epitaxial islands than the islands on the sample viewed in TEM subsequently. Thus, it seems that the size, shape, and uniformity of the surface contamination could be dependent on the amount of time that passes between jet-polishing and TEM usage, as the larger, less uniform particles, such as those in e), have more time to grow than the smaller, more uniform particles, such as those in c) or d). Whether the changes in shape and size of contamination particles on the surface of the Cu-6 wt.% alloy disks over time is caused by a thermodynamic process, such as Ostwald ripening, or a kinetic process is a question that has emerged through the investigation of these surface contamination particles, and will be discussed further in Chapter V.

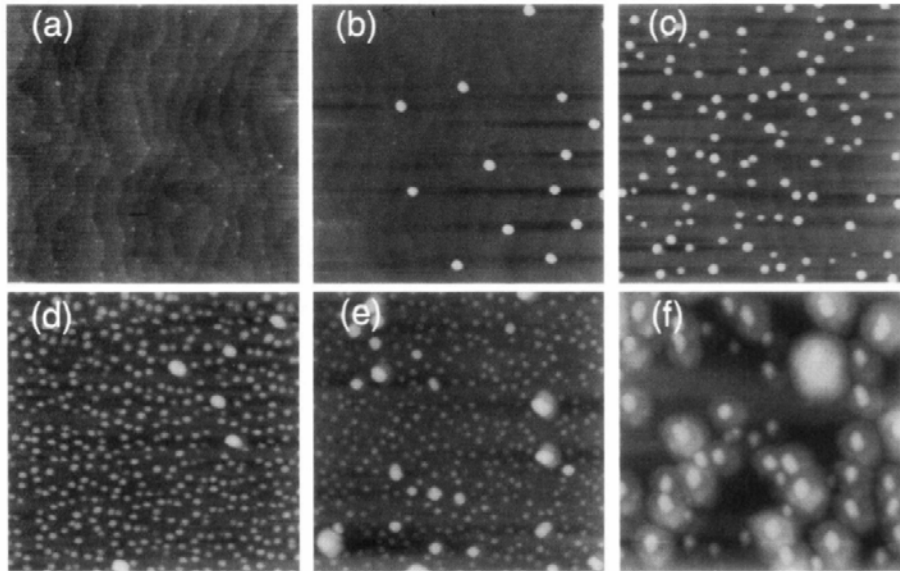


FIG. 1. A series of $1 \times 1 \mu\text{m}^2$ atomic force microscopy images of a range of coverages of InAs on (100) GaAs, from one monolayer in (a) up to four monolayers in (f), produced by use of a Ta shadow mask. The best size uniformity ($\pm 10\%$ in height, $\pm 7\%$ in diameter) of self-assembled islands of InAs is found only at the initial stages of their formation.

Figure 4.2 [27]

4.1.2 Etching of High-Density Crystal Planes

It can be seen in Figure 4.1 g) that there are what appears to be raised lines crossing each other so that parallelogram geometries are formed. Also, it was mentioned previously that one artifact that can occur during the jet-polishing process is the preferential etching of high density crystallographic planes if the voltage during jet-polishing is lower than required for the polishing plateau region [5]. It is possible that these lines are FCC Cu high-density $\{111\}$ slip planes that were preferentially polished before the voltage was adjusted into the plateau region.

Alternatively, these features could be an artifact of an earlier stage of sample preparation. In Figure 4.3, it can be seen that the $\{111\}$ planes form parallelogram shapes, with roughly 60° and 120° angles at the corners, with the crystal lattice.

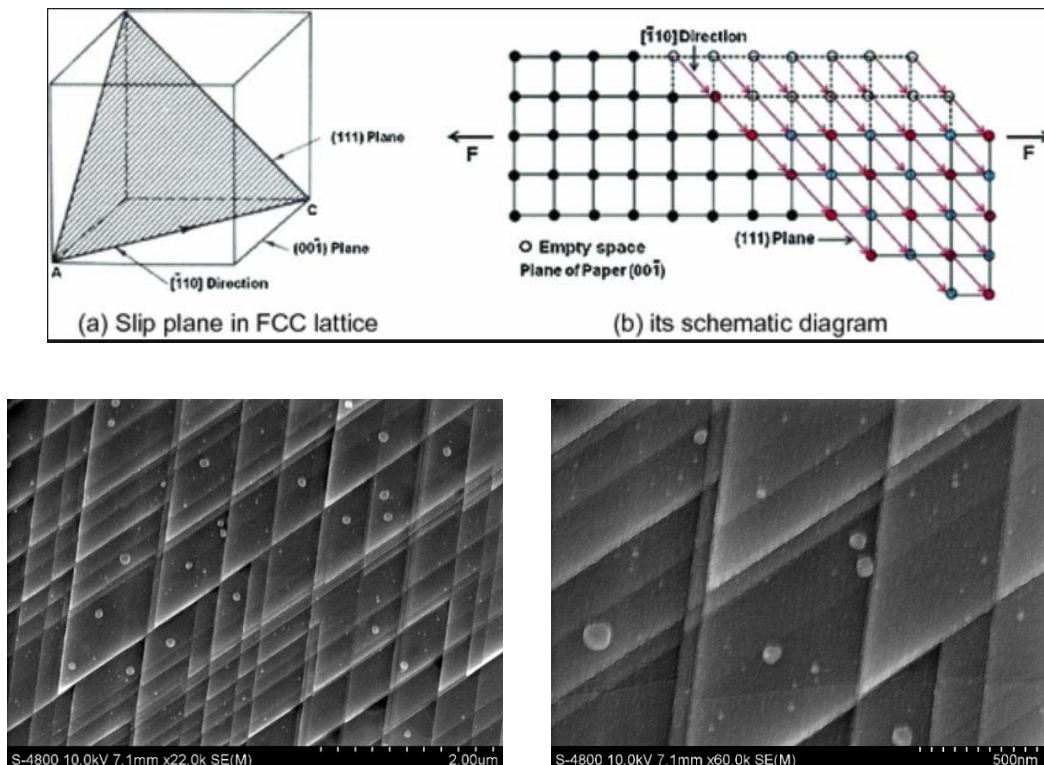
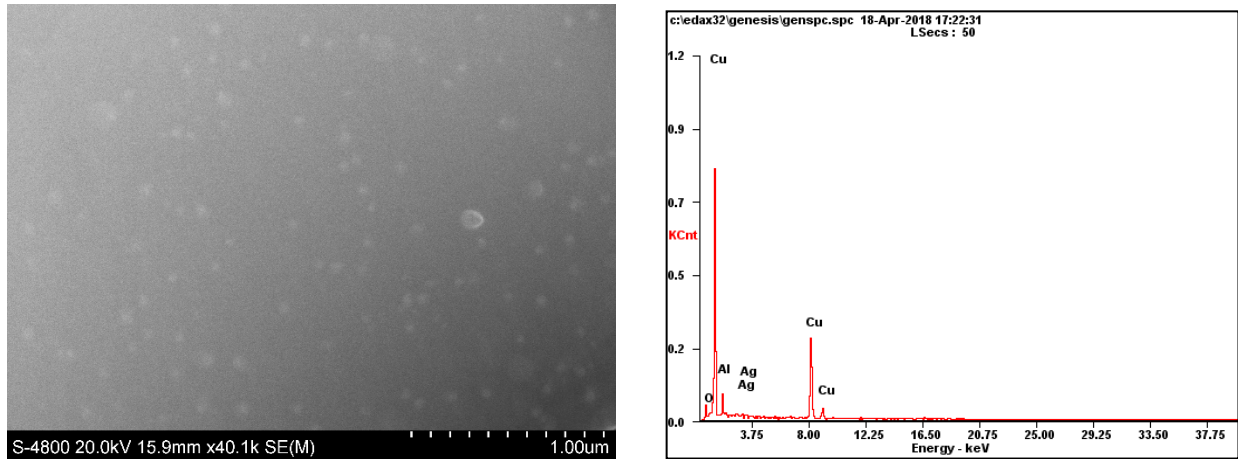


Figure 4.3 [28]

4.2 EDS Analysis Results

As discussed in Chapter III, the EDS analysis performed using the Hitachi S-4800 HR-SEM was difficult due to the limiting factor of the nanometer-scale size of both the sample thickness and the diameter of the surface contamination particles. Due to these factors, the EDS analysis presented here should not serve as an accurate quantitative result, but rather give a qualitative overview about the composition of the surface contamination on the Cu-6 wt.% alloy disks. Both the mapping and spectrum analysis were taken near the perforation created during the jet-polishing process.

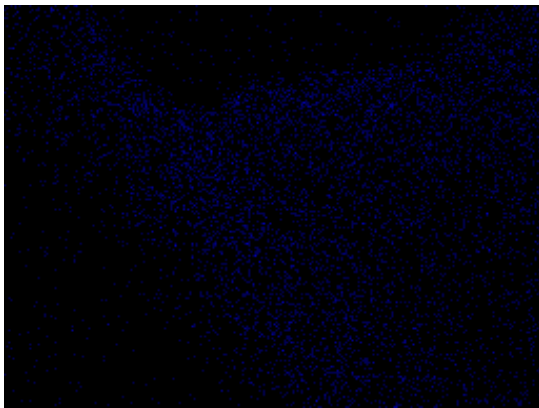
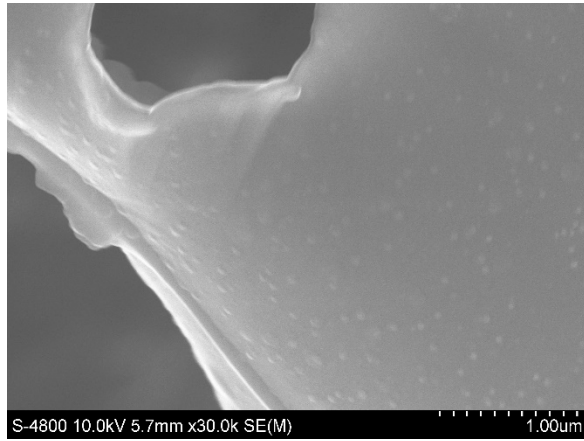
EDS Spectrum Results



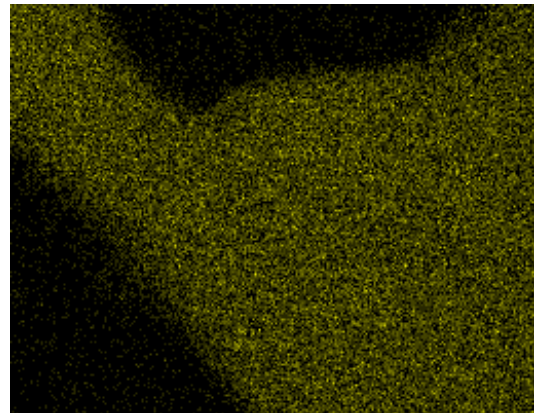
<i>Element</i>	<i>Wt %</i>	<i>At %</i>
<i>OK</i>	02.11	06.67
<i>AlK</i>	14.71	27.65
<i>AgL</i>	02.16	01.01
<i>CuK</i>	81.03	64.67

Figure 4.4

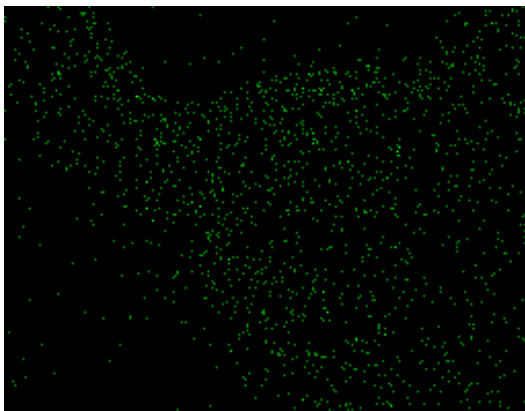
EDS Mapping Result



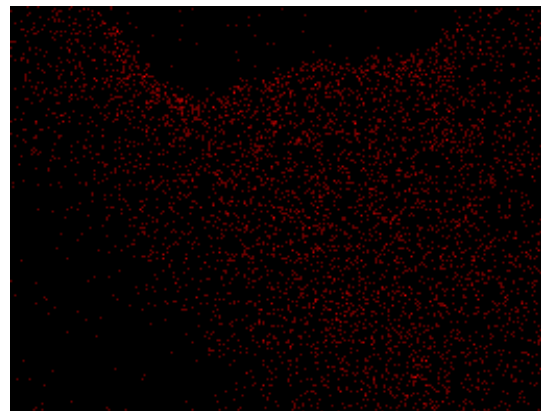
Al K



Cu K



O K



C K

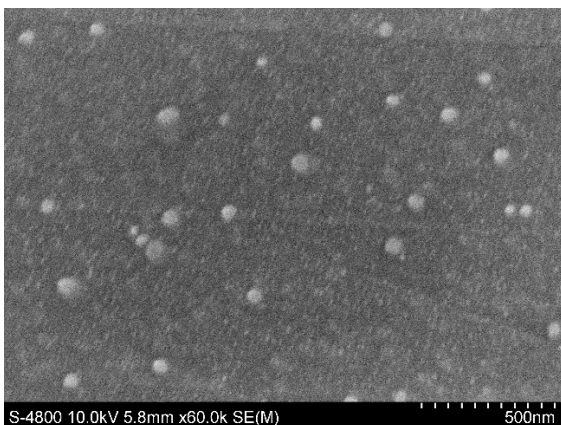
Figure 4.5

In Figure 4.4 and 4.5 showing the results of the EDS line spectrum analysis and the EDS mapping, it is evident that Cu is the element with the largest presence, followed by aluminum and oxygen. It appears that aluminum has a relatively large presence considering its 6 wt.% contribution to the alloy. This fact, along with the presence of oxygen, could add evidence to the suggestion that the surface contamination is originating from the oxide layer that forms during jet-polishing [3, 5]. The outliers in this data are the Ag detected during spectrum analysis and the C detected by mapping analysis. It is possible that these elements could be originating from the jet-polishing process, or simply be inaccurate results caused by the limiting factors of the EDS analysis. Again, these results are meant to give a general idea about the elements present in the samples rather than to provide definitive quantitative results about the amounts of each element.

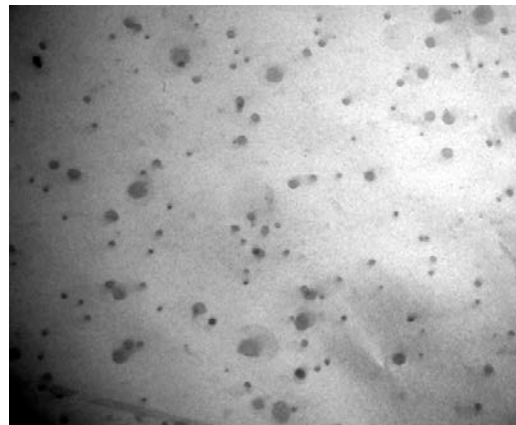
4.3 Comparison of HR-SEM and TEM Images of Contamination Particles

After initial HR-SEM investigation of the contamination particles on the surface of the Cu-6 wt. % alloy disks, the HR-SEM images were compared with TEM images of the same samples. For this comparison, HR-SEM and TEM images of a similar magnification were chosen. The result can be seen in Figure 4.6.

a) 60k-75k X

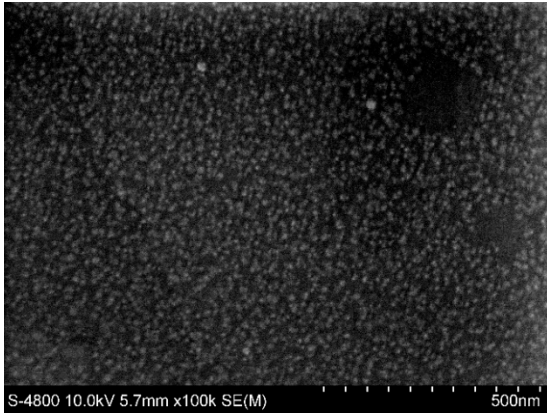


HR-SEM Image at 60k X

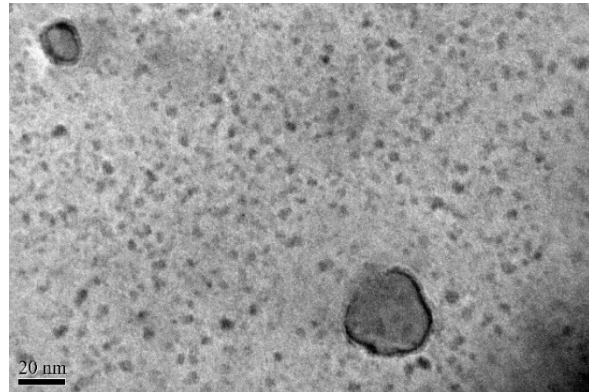


TEM BF Image at 75k X

b) 100k X

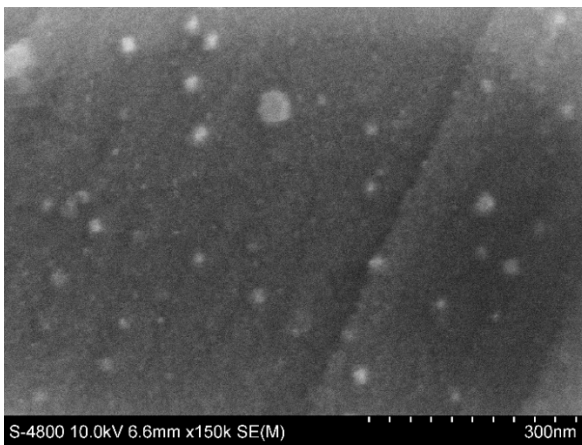


HR-SEM Image at 100k X

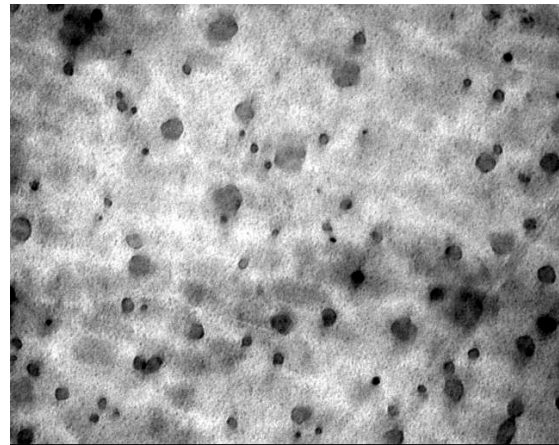


TEM BF Image at 100k X

c) 120k-150k X



HR-SEM Image at 150k X



TEM BF Image at 120k X

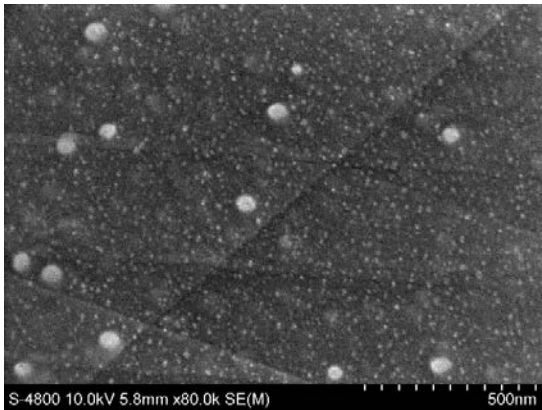
Figure 4.6

From this comparison, it is evident that the shape, size, and distribution of the surface contamination particles seen on the HR-SEM images match well with that of those seen in the original TEM images. Also, as was observed during the initial HR-SEM imaging, the TEM images also seem to show variance in shape and size of the contamination particles among different samples, and among individual samples as well.

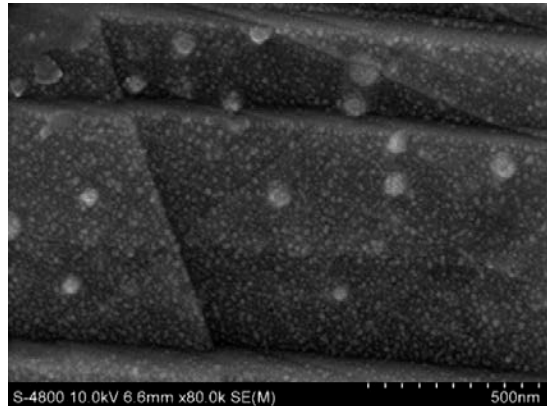
4.4 HR-SEM Results Post-Ion Cleaning

After ion cleaning was performed on the samples for 5 minutes using an Ar ion beam energy of 4 keV and a beam angle of 4° incident to the sample surface, the samples were imaged using HR-SEM to determine if the contamination particles on the surface of the Cu-6 wt. % alloy disks were removed. Figure 4.7 shows a comparison of HR-SEM images for each sample before and after ion cleaning was performed. HR-SEM images of similar magnifications were chosen for the before and after comparison images so that an accurate determination could be made about the effect that ion cleaning had on the contamination particles.

a) As Quenched: Sample 1

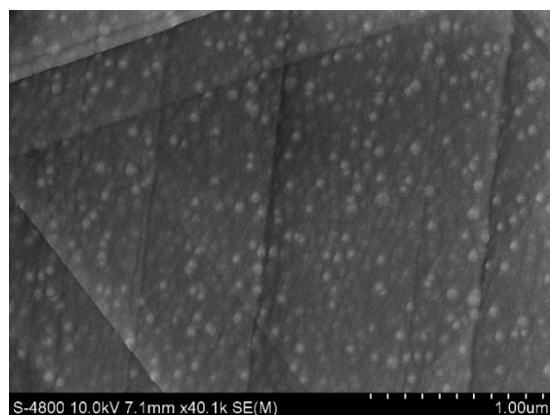
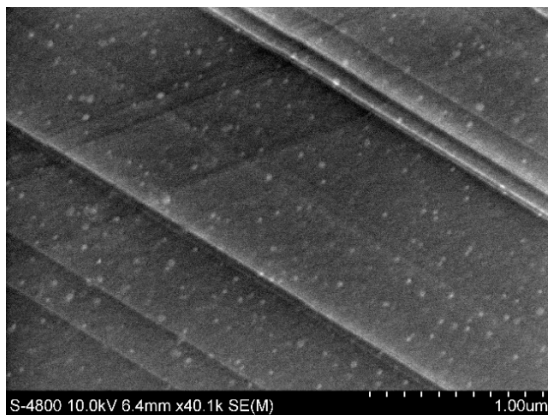


Before Ion Cleaning



After Ion Cleaning

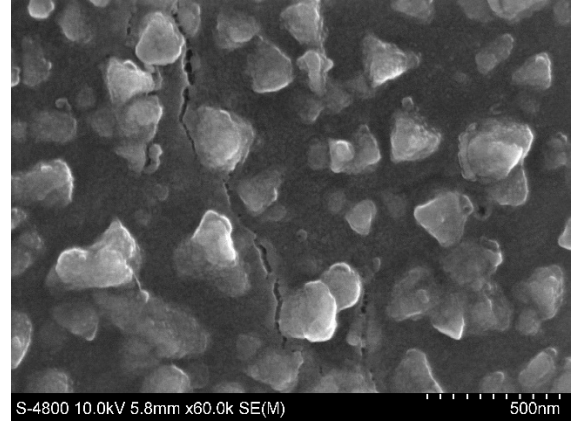
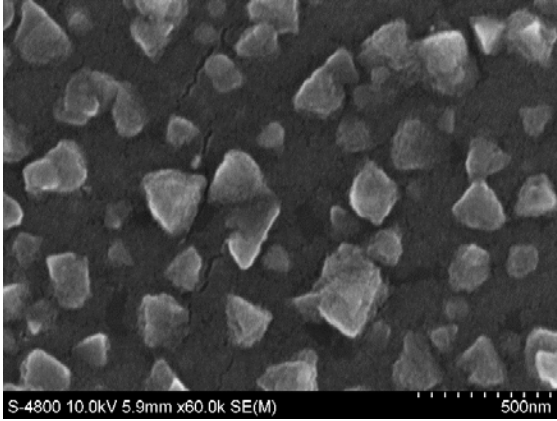
b) As Quenched: Sample 2



Before Ion Cleaning

After Ion Cleaning

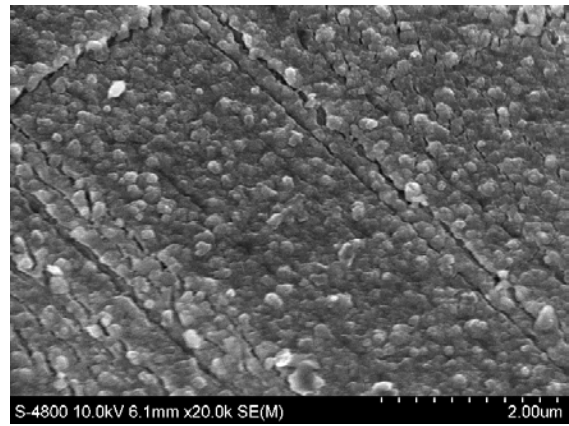
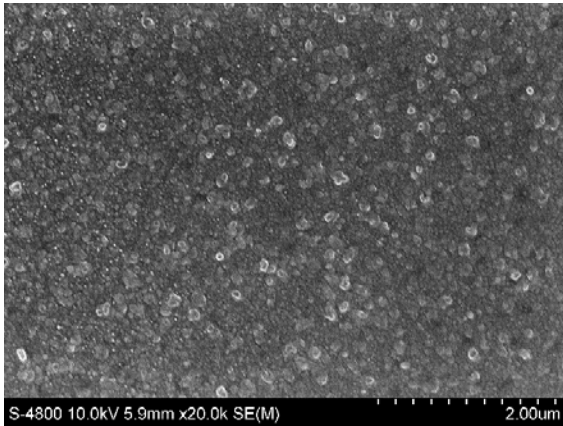
c) Aged at 250° C for 28 Days: Sample 1



Before Ion Cleaning

After Ion Cleaning

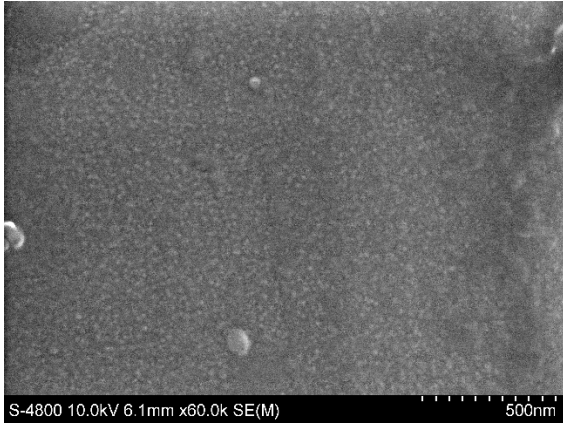
d) Aged at 250° C for 28 Days: Sample 2



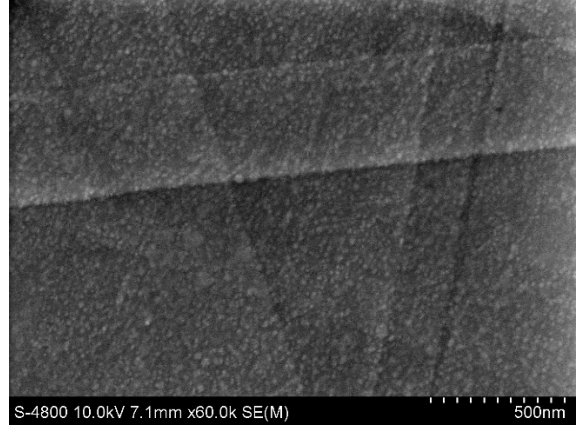
Before Ion Cleaning

After Ion Cleaning

e) Aged at 950° C for 1 Hour: Sample 1

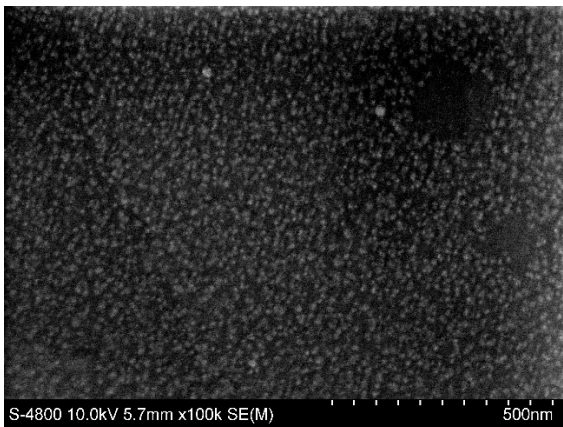


Before Ion Cleaning

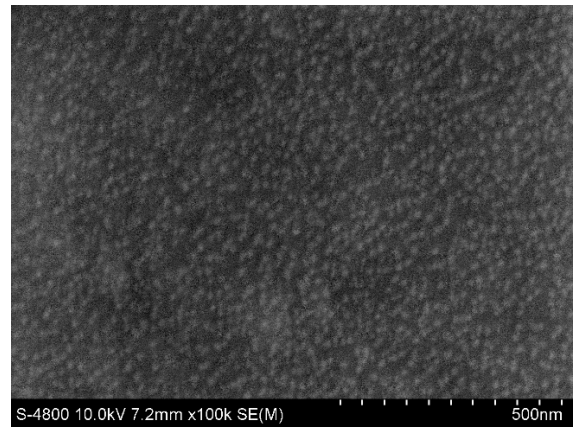


After Ion Cleaning

f) Aged at 950° C for 1 Hour: Sample 2

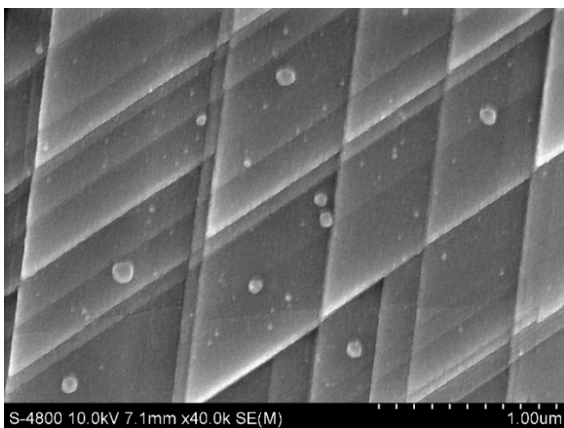


Before Ion Cleaning

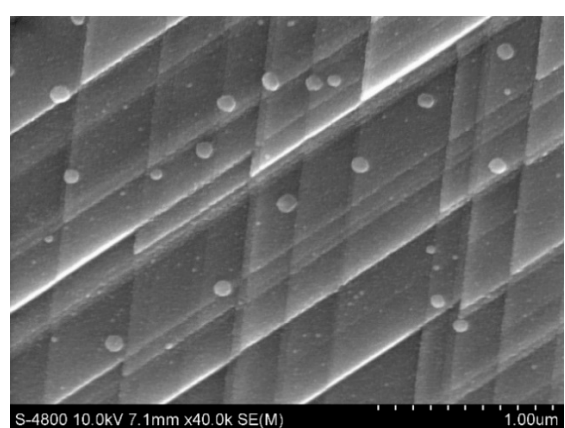


After Ion Cleaning

g) Aged at 450° C for 19 Hours: Sample 1



Before Ion Cleaning



After Ion Cleaning

Figure 4.7

It can be seen in Figure 4.7 that ion cleaning was not successful in removing the contamination particles from the surface of the Cu-6 wt. % alloy disks. Further, in comparison with the contamination particles seen in the HR-SEM images before ion cleaning was done, the contamination particles appear essentially unchanged in the HR-SEM images taken after ion cleaning was performed on the samples. It is possible that the ion cleaning method could be modified, by adjusting the operational parameters used in the experiment, in such a way that the contamination particles could be removed from the surface of the TEM disks. A summary of the results presented in this chapter and discussion about potential future experiments is given in Chapter V.

CHAPTER V

DISCUSSION, FUTURE RESEARCH, AND CONCLUSIONS

5.1 Summary of Results and Discussion

This thesis research began with two main objectives in mind, with the first being to characterize the surface contamination particles previously seen on TEM images of the Cu-6 wt.% Al alloy disks. HR-SEM was chosen to identify the particles, and to characterize them in terms of shape, size, and composition. As was discussed in Chapter II, the EDS composition spectrum and mapping analysis was complicated by the nanometer-scale size of the particles, the thin nature of the samples, and limiting operational factors of the EDS attachment [23]. Rather than providing accurate quantitative data, results of the analysis were only useful to the extent of giving a general idea about the different elements present in the sample. However, the HR-SEM characterization of the particles with respect to shape and size was successful in few different aspects. Since the surface contamination particles were discovered incidentally as other characteristics of the Cu-6 wt.% Al alloy were being investigated with TEM, a thorough analysis of the particles was not completed in previous research. Further, of the seven TEM disks of the alloy studied in this research, TEM analysis was not performed on all of the samples after preparation via jet-polishing. Thus, HR-SEM imaging and analysis was successful in confirming that contamination particles are present on the surface of the Cu-6 wt.% Al alloy disks regardless of aging temperature or duration.

Once the surface contamination particles on the Cu-6 wt.% Al alloy disks were characterized with HR-SEM, the next objective of this research was to use low-angle ion milling to remove the particles. As discussed in Chapter II, ion milling was chosen as a possible

technique for removing the particles because of its capacity to sputter material from the surface of a sample [2-3,6]. However, as can be seen in the HR-SEM images of the TEM disks taken after ion milling was done, the contamination particles remained on the surface of the Cu-6 wt.% Al alloy TEM disks. Since ion milling was unsuccessful in removing the surface contamination particles, the goals of this research shifted from characterizing and attempting to remove the particles to suggesting mechanisms to explain certain behaviors and characteristics of the surface contamination particles observed during the initial stages of this research. First, while the TEM images revealed spherically shaped particles on the surface of the alloy disks, the HR-SEM characterization revealed a variance in the shape and size of the contamination particles. Suggesting a possible mechanism responsible for the variation in shape and size of the particles became a secondary aim of this research. Additionally, since previous TEM analysis showed that the particles were growing epitaxially on the Cu matrix, suggesting a possible mechanism for how this process is occurring at low-temperatures in an electrolyte also became a secondary goal of this research. Although these questions were addressed in previous chapters, further discussion is given in the following sections, as well as suggestions for future research and potential experiments.

5.1.1 Epitaxial Growth Occurring in an Electrolyte

A background on kinetically driven and thermodynamically driven epitaxial growth modes was given in Chapter II, but a discussion of how it is possible that the contamination material on the surface of the Cu-6 wt.% Al alloy TEM disks is growing epitaxially on the Cu matrix in an electrolyte at low temperature was not addressed. The aim of this section is to show that a 3D growth mode, suggested in Chapter II as the possible mechanism behind the epitaxial

growth of the redeposition material on the Cu-6 wt.% Al alloy TEM disks, is possible in a low-temperature electrolyte.

Generally, epitaxy is performed in a high-vacuum environment at high temperatures to ensure that the material deposited onto the surface of the material grows as an atomically flat thin film. In other words, the preferred epitaxial growth mode of material deposited on the surface of a substrate is either the thermodynamically driven Frank-van der Merwe or Stranski-Krastanov modes or the kinetically driven step-flow or layer-by-layer modes [15-16]. Obtaining high-quality thin film/substrate materials created for industry or research use using a high-vacuum system is an expensive process. However, a few papers note that it is possible to achieve high quality, epitaxially-grown metallic thin films using an electrodeposition process [29-30]. These papers were of interest to this thesis research due to their discussion of epitaxial growth occurring in an electrolyte and were reviewed in the context of answering two major questions that were raised during this research: “How does epitaxial growth occur in an electrolytic environment?” and “What is the mode of epitaxial growth that is occurring in these conditions?” Below follows a summary of these studies and a discussion of their findings in the context of these questions.

Sieradzki et. al [29] developed a way to produce high quality 2D epitaxially grown films using an electrodeposition process. The authors of this study named this method electrochemical defect-mediated growth, or DMG. While the epitaxial growth of Ag on Ag and Au at room temperature is usually controlled by a 3D epitaxial growth mode, the goal of their study was to create 2D epitaxial thin films of Ag on the substrates of Au (111) and Ag (111). They note that the difficulties generally associated with the growth of 2D epitaxial films by electrodeposition and room-temperature high vacuum techniques are due to kinetic issues. That is, due to energy

barriers at low-temperatures, atoms tend to assume a 3D growth mode rather than 2D layer-by-layer growth. The authors explain that in order for 2D growth layer-by-layer growth to commence, the transport and diffusion of atoms between layers of growth must occur very rapidly. As discussed in Chapter II, this is difficult to achieve at low temperatures because the atoms must overcome an energy barrier in descending the step to the layer below [15-16]. The paper states that the frequency of attempts by the atoms to descend to the step below is given by:

$\frac{D}{L^2}$, where D is the diffusivity of the atoms and L is length factor describing the size of the island.

Since diffusivity increases with temperature, it can be seen from this equation that a high temperature growth environment will lead to a larger frequency of atoms attempting to descend island steps, and thus a higher probability that epitaxial growth will occur via 2D layer-by-layer growth. At low temperatures, instead of descending the islands and coalescing on the layer below, the atoms remain on the island, attach to one another, and nucleate smaller islands, eventually leading to 3D growth [15-16]. The authors of the study reference analytical arguments which predict that a critical radius of 2D islands determines whether the islands transition to a 3D epitaxial growth mode or grow layer-by-layer. The predicted critical radius is on the order of $\left(\frac{4a^2D}{J}\right)^{1/6}$, where a represents the distance an atom must jump to its nearest neighbor and J represents the deposition flux of atoms onto the substrate. These arguments suggest that layer-by-layer growth will occur when the radius of the 2D islands is larger than the distance between islands [29]. Conversely, it should logically follow that 3D growth will occur if the radius of the 2D islands is less than the distance between islands.

The DMG method created by Sieradzki et. al was successful in growing atomically flat, epitaxial thin films for the Ag/Ag (111) and Ag/Au (111) thin film/substrate systems. Through

DMG, the researchers deposited Ag atoms and “mediator” atoms onto the surface of Ag and Au substrates. The mediator atoms, Pb and Cu used in separate experiments, were simultaneously deposited onto the substrate with the Ag atoms. The purpose of the mediator atoms was to provide a structure by which the Ag atoms could nucleate 2D islands. After a short time, the potential of the electrodeposition system was manipulated, causing reverse deposition and removing the mediator atoms from the surface of the substrate, leaving the 2D Ag islands. This process was repeated several times, with the mediator atoms allowing a large number of 2D Ag islands to nucleate and coalesce as full layers on the substrate [29]. An illustration from the paper explaining the DMG method is shown in Figure 5.1

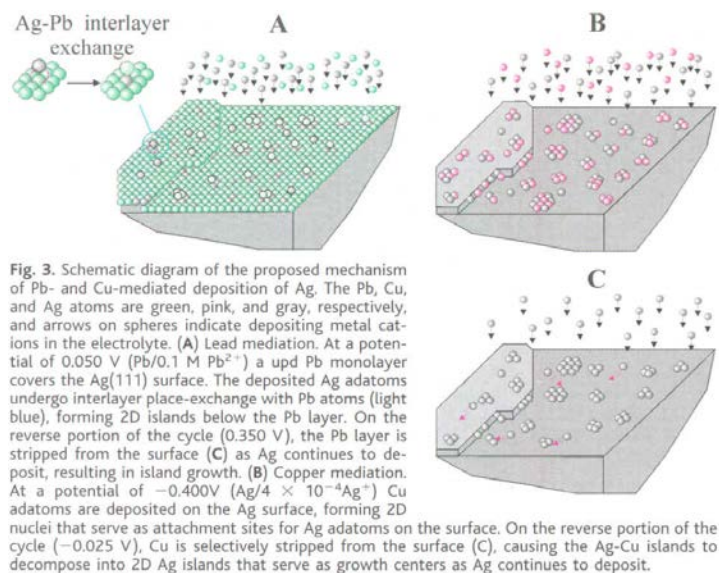


Figure 5.1 [29]

Additionally, a study by Hwang et. al [30] used the DMG method created by Sieradzki et. al [29] to induce layer-by-layer epitaxial growth of Cu on an Au (111) substrate using Pb mediator atoms. The study used scanning tunneling microscopy (STM) to take in-situ images of

the epitaxial growth of the Cu atoms on the Au (111) substrate. After growing the epitaxial film to around 80 nm via DMG, the researchers confirmed the epitaxial growth by performing XRD on the samples. The XRD results showed Au (111), Cu (111), Au (222), and Cu (222) peaks, thus confirming the epitaxy. Figure 5.2 shows the STM images from the Hwang et. Al study compared with an HR-SEM image of the surface contamination investigated in this research. It can be seen in this comparison that the shape and size of contamination particles on the surface of the Cu-6 wt. % Al disks match well in terms of shape and size with the epitaxially grown Cu islands seen in Image A. of the STM images taken by the Hwang et. Al study. The study notes that the epitaxial island form of the Cu atoms seen in Figure 1 A. was due to slow deposition of the Cu through the electrolyte, perchlorate [30]. Image A. of the STM images from the Hwang et. al study is of interest to this research because it represents the epitaxial growth of deposition material occurring in an electrolyte before the DMG process has begun in earnest. Figure 1A in the Hwang et. al study in Figure 5.2 shows an example of what the initial stages of epitaxial growth might look like in a low temperature electrolytic environment without the assistance of mediator atoms [30].

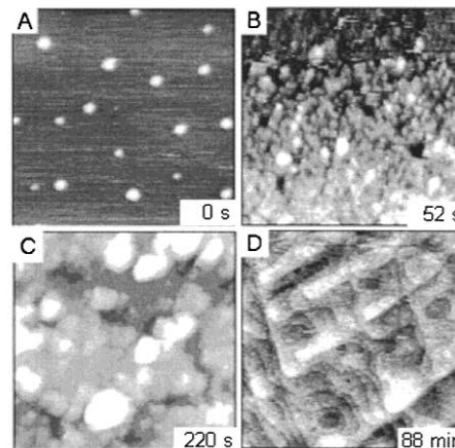
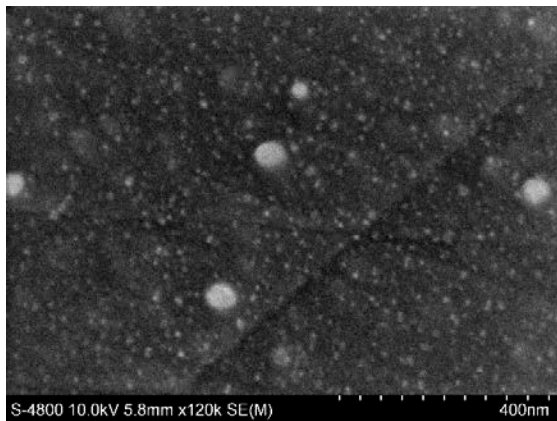


Figure 1. A temporal sequence of in situ STM images of Cu electrodeposition on Au(111) with Pb mediator. (a) 149 nm × 149 nm image of the initial stage of Cu upd on Au(111) terrace. Growth of Cu adlayers after (b) two 1-s pulses to 0.050 V and (c) 6 pulses. Acquisition time of (a–c) was 42 s. (d) Thicker Cu film (ca. 100 ML which was measured by stripping voltammetry) after 2000 pulses. (380 nm × 380 nm) At the lower right corner is shown the time at which scan started. In all images, the y-scan direction is downward.

Figure 5.2 [30]

The point in reviewing these studies for this research is not to suggest that the epitaxial growth of the surface contamination on the Cu-6 wt. % Al disks is occurring by the same mechanisms discussed in these studies. After all, the epitaxial growth conditions for the surface contamination particles studied in this research and the growth conditions of the Ag and Cu films in the Sieradzki et. al study and the Hwang et. al study, respectively, are quite different. First, in these two studies, electrodeposition is the method used to deposit atoms onto the substrate material. In electrodeposition, positively charged metal ions are deposited on a negatively charged cathodic substrate. Conversely, the epitaxial growth of the surface contamination particles on the Cu-6 wt. % Al disks is occurring on a positively charged anodic substrate. Second, the epitaxial growth of the Ag and Cu films in these studies is occurring with the help of mediator atoms, while the surface contamination particles on the Cu-6 wt. % Al disks are not. Thus, as stated above, the goal in reviewing these studies here is not to suggest that the mechanisms governing the epitaxial growth of the surface contamination particles on the Cu-6

wt. % Al disks and the Ag and Cu epitaxial films in these studies are the same, but rather to answer the questions posed at the beginning of this section, “How does epitaxial growth occur in an electrolytic environment?” and “What is the mode of epitaxial growth that is occurring in these conditions?”. The review of the Sieradzki et. al and Hwang et. al study answers these questions in that they suggest that epitaxial growth is possible in an electrolytic environment and that atoms tend to grow in a 3D epitaxial manner in this environment without control from a process such as DMG [29-30].

5.1.2 Particle Coarsening (Ostwald Ripening)

Generally, particle coarsening, also known as Ostwald ripening, is a process used to describe a phenomenon that occurs in two-phase alloys in which a high density of small precipitates undergoes coarsening, resulting in a low density of large precipitates. This process is driven by the fact that if the total interfacial free energy is not minimum, the microstructure of a two-phase alloy is not stable. Because particle coarsening is dependent of the size and distribution of precipitates in a solid solution, the mechanisms driving this process could be extended to describe the difference in shape and size of the contamination particles seen on the surface of the Cu-6 wt.% Al TEM disks [31]. Figure 5.3 shows the difference in shape and size of the surface contamination particles alongside a basic illustration of particle coarsening.

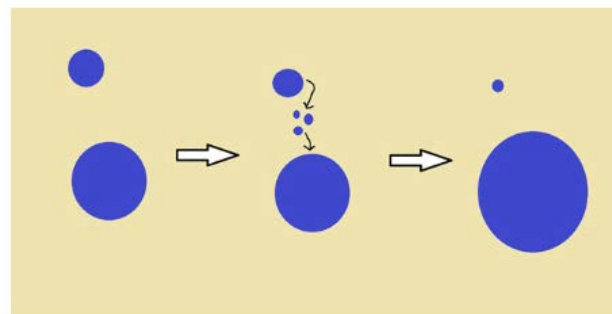
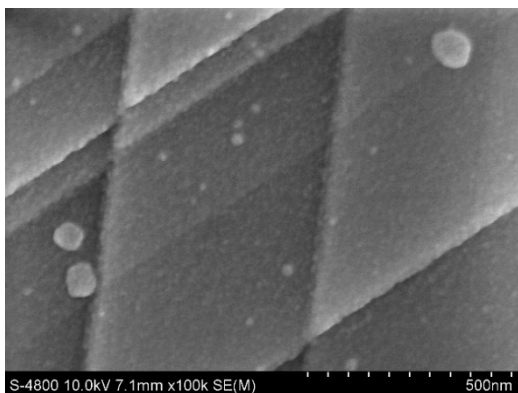


Figure 5.3 [32]

Particle coarsening is a thermodynamically driven process that occurs due to the Gibbs-Thompson effect. Precipitates in two-phase alloys nucleate and grow at different rates, which results in differences in particle size among the precipitates. Similarly, the contamination particles on the surface of the Cu-6 wt.% Al TEM disks appear to have grown epitaxially in such a way that has caused the particles to have different sizes. According to the Gibbs-Thompson effect, the solute concentration in the matrix of a two-phase alloy will increase as the radius of curvature decreases. Thus, the solute concentration will be large surrounding small particles with a small radius of curvature, while the solute concentration will be small surrounding large particles with a large radius of curvature. The free energy vs. concentration curves for the Gibbs-Thompson effect can be seen in Figure 5.4. This effect causes concentration gradients in the matrix of the two-phase material between small particles and large particles. The solute will diffuse along the concentration gradients from the large solute concentration surrounding the small particles to the small solute concentration surrounding the larger particles. Over time, the larger particles become larger while the smaller particles shrink, and there will be a reduction in the total number of particles.

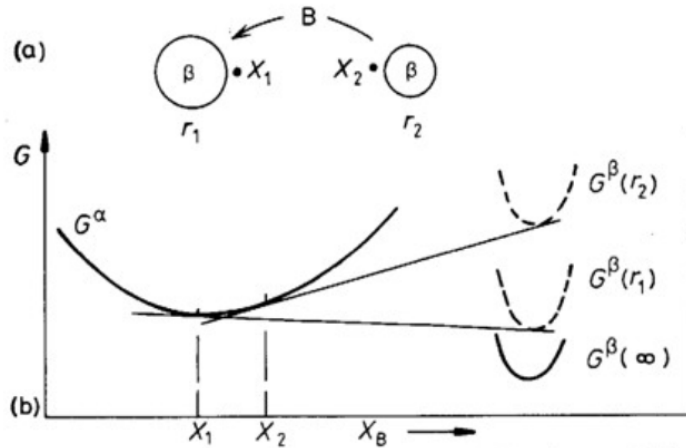


Fig. 5.43 The origin of particle coarsening. β with a small radius of curvature (r_2) has a higher molar free energy than β with a large radius of curvature (r_1). The concentration of solute is therefore highest outside the smallest particles.

Figure 5.4 [31]

The pioneers of particle coarsening theory, C. Wagner, I. M. Lifshitz, and V.V. Slyovov, showed that particle coarsening should behave according to the following relationship [31]:

$$(r)^3 - r_0^3 = kt$$

where $k \propto D\gamma X_e$,

r_0 is the average particle radius size at $t=0$, and r is the average particle radius at a given time after $t=0$. For the k factor equation, D is the diffusion coefficient, X_e is the equilibrium solubility of large particles, and γ is the interfacial free energy. The k factor is dependent on temperature since D and X_e increase with temperature. Thus, particle coarsening is a process that is dependent on both temperature and time. If particle coarsening is the process causing the observed shape and size difference of the surface contamination particles on the Cu-6 wt.% Al TEM disks, it is occurring either in the low temperature conditions of the jet-polishing cell or in ambient room temperature conditions after the jet-polishing has been performed. Thus, given these low-temperature conditions, it is likely that the possible particle coarsening of the surface contamination particles would occur at a slow rate over an extended period of time [31].

At this point, the issues with using particle coarsening to describe the difference in shape and size of the contamination particles is that the composition of the particles is unknown. The composition of the surface contamination particles must be known in order to validate particle coarsening as the process behind the size difference of the particles. This is due to the fact that particle coarsening is a process that is based on the assumption that the particle is composed of a solute material or, if the particle is a precipitate, that it is composed of a different phase than the bulk material. Additionally, the average radius of the particles must be measured at time zero and again after a certain time interval. Thus, though it is plausible as a mechanism for the observed shape and size difference of the surface contamination particles on the Cu-6 wt.% Al alloy TEM disks, this prediction requires further study before it can definitively be said that it is the mechanism causing the observed phenomenon. Suggestions for potential experiments are discussed in the following section [31].

5.2 Future Research and Potential Experiments

The results of this thesis research raised several questions about the nature of the contamination on the surface of the Cu-6 wt.% Al alloy TEM disks occurring during jet-polishing. The suggestions made as to the possible mechanisms causing the observed behavior of the surface contamination cannot be fully explored or validated without further investigation and knowledge, and thus a discussion of potential experiments is given here.

One experiment, which is a direct extension of this thesis research, would be to perform low-angle ion milling on the samples using different operational parameters than those used in this research. Although ion milling was unsuccessful in removing the contamination particles from the surface of the Cu-6 wt.% Al alloy disks, it is possible that adjusting the beam energy, beam angle, and the ion milling duration time could result in the removal of the contamination

particles. In this research, ion milling was performed for five minutes using a beam energy of 4keV and a beam angle of 4° incident to the sample surface. Increasing the ion milling time to ten minutes, and selecting a larger beam energy and beam angle, such 6 keV and 6° incident to the sample surface, respectively, might be successful removing the contamination particles from the surface of the samples. Because a few studies report that ion milling was successful in removing surface contamination from electropolished TEM disks, the method should be reconsidered, using different operational parameters, as a technique for removing the surface contamination from the jet-polished Cu-6 wt.% Al TEM samples [2,9].

An important question regarding the nature of the surface contamination on the Cu-6 wt.% Al TEM disks is whether a film of contamination material exists on the surface of the samples below the contamination particles seen on the HR-SEM images. Also, it is important to determine the composition of such a film, if it exists, and to determine the composition of the surface contamination particles themselves. Of the studies mentioned in Section 2.3.1, all of which report surface contamination in electropolished TEM samples of Al-based Cu alloys and Cu-based Al alloys, most used XPS to identify the existence of a thin film of solute material on the surface of the TEM samples being investigated [9-12]. X-ray photoelectron spectroscopy (XPS) is a characterization method that can be used to determine the elemental or chemical composition of the surface of a sample. XPS uses X-rays of a known energy, such as Al $K\alpha$ X-rays, to probe the surface of a sample to a depth of around 10 nm. Electrons are emitted from the surface of the sample and their kinetic energy is recorded. The composition of the sample is determined by determining the electron binding energy, which is characteristic of both the element and the specific electron shell from which the electron originates. The electron binding energy is given by the following equation:

$$E_{binding} = E_{X-ray} - (E_{kinetic} + \phi)$$

ϕ is a work function that is dependent on both the XPS machine and the material being studied. The XPS software produces a plot showing the intensity of each detected electron binding energy (counts) vs the characteristic binding energies. In this way, the elements present on the surface of sample and the relative amount of each can be determined [20]. XPS could be performed with the Cu-6 wt.% Al TEM disks to determine if a film is present on the surface of the samples and to determine the composition of the surface contamination particles. Knowledge of whether an epitaxially grown thin film of redeposition material is present on the surface of the TEM disks would be useful in the further study on the possible growth mode governing the epitaxial nature of the surface contamination observed in this alloy. Additionally, knowledge of the composition of the surface contamination particles could also help in the study of the observed epitaxial growth and also in determining whether particle coarsening is occurring on the surface of the samples.

It can be seen in Chapter IV that the shape and size of the surface contamination particles varies among the different samples and sometimes shows this variation in shape and size on a single sample. One mechanism that can be used to explain this effect is particle coarsening, or Ostwald ripening, which is a thermodynamically driven process in which large particles grow at the expense of smaller particles [31]. This phenomenon is discussed in the previous sections of this chapter. One way to test these theories would be to perform jet-polishing, using all the same parameters that were used in the previous experiments, with new Cu-6 wt.% Al TEM disks. All samples could be imaged with HR-SEM immediately after jet-polishing to establish a baseline reference for the shape and size of the contamination particles. Then, the samples could be imaged again after selected time intervals, such as a few days, to observe and record changes in

the shape and size of the particles. Along with the knowledge of the composition of the surface contamination particles, this potential experiment could lend valuable knowledge to the study of the possible particle coarsening of the surface contamination particle on the surface of the Cu-6 wt.% Al TEM disks. With known factors such as the composition of the particles, the temperature of the environment, a measured time interval, and the average radius of the particles at the beginning and end of this time interval, it could be possible to determine if particle coarsening is the process controlling size difference of the surface contamination particles.

5.3 Conclusions

After previous experiments by our group determined that the particles seen growing epitaxially on the surface of the Cu-6 wt.% Al TEM disks were surface contamination particles rather than precipitates, several questions emerged as to how the process was occurring and why the surface contamination particles presented with certain characteristics. This research has attempted to suggest possible mechanisms by which the contamination is growing epitaxially on the surface of the disks and has predicted particle coarsening as a possible explanation for the observed shape and size difference of the particles. The mechanisms discussed to explain these phenomena require further study and experiments, but perhaps the suggestions for potential experiments detailed in this chapter will lead to a better understanding of the epitaxial growth of surface contamination on jet-polished TEM samples and will help to determine if particle coarsening is occurring on the surface of the samples.

Although ion cleaning was unsuccessful in removing the surface contamination particles from the Cu-6 wt.% Al TEM alloy disks, the success of this thesis research lies in its potential to bring increased awareness to the issue of surface contamination occurring during the jet polishing process. As was discussed in previous chapters, successful preparation of high quality,

contamination-free TEM disks via jet-polishing is subject to the correct choice of several operating parameters. Because of the large number of operating parameters that must be carefully chosen and the fact that the knowledge of the correct polishing parameters for a specific alloy is often gained experimentally, the jet-polishing process has the potential for several errors in the choice of operating parameters than can lead to various types of surface contamination on the polished TEM disks. The hope is that this research will enable future studies and experiments to recognize the presence of surface contamination in jet-polished TEM samples and avoid the misinterpretation of TEM data that can be caused by assuming that this surface contamination is true microstructure.

REFERENCES

1. Choong-Un Kim, "Characterization", Lecture Handout for Analysis of Materials Course, The University of Texas at Arlington: Department of Materials Science and Engineering, Fall 2016.
2. D. V. Sridhara Rao, K. Muraleedharan, and C. J. Humphreys, "TEM specimen preparation techniques", *Microscopy: Science, Technology, Applications and Education*, Vol. 2, pp. 1232-1244, 2010.
3. D. B Williams and C.B. Carter, "Transmission Electron Microscopy: A Textbook for Materials Science", Springer, New York, 1996.
4. L. A. Bendersky and F. W. Gayle, "Electron Diffraction Using Transmission Electron Microscopy", *J Res Natl Inst Stand Technol*, Vol. 106(6), pp. 997-1012, 2001.
5. J. Ayache, L. Beaunier, J. Boumendil, G. Ehret, and D. Laub, "Sample Preparation Handbook for Transmission Electron Microscopy", Springer, New York, 2010.
6. P. J. Lee, "Enhanced Control of Electropolishing for the Preparation of Thin Foils for Transmission Electron Microscopy: Artificial and Multiple Phase Micro-Electropolishing", *Proc. Microscopy & Microanalysis '96*, ed. G. W. Bailey et al., San Francisco Press, pp. 1028-1029, 1996.

7. R. Rokicki and T. Hryniewicz, "Enhanced oxidation-dissolution theory of electropolishing", Transactions of the Institute of Metal Finishing, Vol. 90(4), pp. 188-196, 2012.
8. V. Palmieri, "Fundamentals of Electrochemistry-The Electrolytic Polishing of Metals: Application to Copper and Niobium", National Institute of Nuclear Physics and University of Padua: Department of Materials Science and Engineering.
9. P.L. Morris, N.C. Davies, and J.A. Treverton, "Effects of a Surface Film Upon Thin Foil Microanalysis", Developments in Electron Microscopy and Analysis, 1977: Proceedings of the Institute of Physics EMAG 77 conference, pp. 377-380, 1977.
10. Z. Luo, "A Practical Guide to Transmission Electron Microscopy, Volume 1: Fundamentals", Momentum Press, New York, 2015.
11. D. Jones, "Principles and Prevention of Corrosion" 2nd Edition, Prentice Hall, Upper Saddle River, NJ, 1996.
12. Eds. J. J. Hren, J. I. Goldstein, and D. C. Joy, *Principles of Analytical Electron Microscopy*, pp. 141-142, Springer US, 1986.
13. L. Zang, MSE 5034 (Kinetics) "Lecture 30: Kinetics of Epitaxial Growth: Surface Diffusion and Nucleation", The University of Utah: Department of Materials Science and Engineering, 2017.

14. J. Palisaitis and R. Vasiliauskas, “Epitaxial growth of thin films”, Physics of Advanced Advanced Materials Winter School 2008, Linköping University, Sweden, 2008.
15. H. Brune, “Epitaxial Growth of Thin Films”, Surface and Interface Science Vol. 4, Chapter 20, pp. 421-477, Wiley Online Library, 2014.
16. H. Brune, “Growth Modes”, Encyclopedia of Materials: Science and Technology, pp. 3683-3693, Elsevier Science Ltd., 2001.
17. M. Jalochoowski, M. Hoffmann, E. Bauer “Low-Temperature Epitaxial Growth of Thin Metal Films: In Situ Electrical Resistivity Study”, *Surface Diffusion*, NATO ASI Series (Series B: Physics), Vol 360. Springer, Boston, MA.
18. J. Evans, D. Sanders, P. Thiel, and A. DePristo, “Low-temperature epitaxial growth of thin metal films”, Physical Review B, Vol. 41(8), pp. 5401-5413, 1990.
19. K. Caspersen, M. Li, J. Evans, C. Stoldt, A. Layson, E. Cox, and C. Chung, P. Thiel, PowerPoint :“Atomistic Models For Low-Temperature Epitaxial Growth of Metal Films”, Iowa State University.
20. Y. Leng, “Materials Characterization: Introduction to Microscopic and Spectroscopic Methods” 2nd Edition, John Wiley & Sons, Incorporated, Hoboken, NJ, 2013.
21. R.F Egerton, “Physical Principles of Electron Microscopy: An Introduction to TEM, SEM, and AEM”, Springer, Boston, MA, 2005

22. D. Brandon and W.D Kaplan, “Microstructural Characterization of Materials”, John Wiley and Sons, New York, 1999.
23. eds. W. Zhou and Z.L. Lang, “Scanning Microscopy for Nanotechnology: Techniques and Applications”, Springer, New York, 2006.
24. “Mechanisms of emission of secondary electrons, backscattered electrons, and characteristic X-rays from atoms of the sample” Image (Figure 2.17), Wikipedia, Wikimedia Foundation, 14 Aug. 2018, https://en.wikipedia.org/wiki/Scanning_electron_microscope
25. “Principle of EDS” Image (Figure 2.18), Wikipedia, Wikimedia Foundation, 14 Aug. 2018, https://en.wikipedia.org/wiki/Energy-dispersive_X-ray_spectroscopy
26. “Scanning Electron Microscopy & Energy Dispersive X-Ray Spectroscopy” Image, (Figure 3.2), VUB: Research Group Electrochemical and Surface Engineering, 14 Aug. 2018, <https://www.surfgroup.be/semedx>
27. D. Leonard, K. Pond, P.M. Petroff, “Critical layer thickness for self-assembled InAs islands on GaAs”, *Physical Review B*, Vol. 50, Number 16, pp. 687-692, October 1994.
28. S. Woo, “Mechanical System Failures: Reliability Design of Mechanical Systems”, Springer, Cham, 2017.
29. K. Sieradzki, S. R. Brankovic, and N. Dimitrov, “Electrochemical defect-mediated thin-film growth”, *Science*, Vol. 284, Iss. 5411, pp. 138-141, 1999.

30. S. Hwang, I. Oh, and J. Kwak, "Electrodeposition of Epitaxial Cu(111) Thin Films on Au(111) Using Defect-Mediated Growth", J. Am. Chem. Soc., Vol. 123 (9), pp. 7176-7177, 2001.
31. D. Porter, K. Easterling, M. Sherif, "Phase Transformation in Metals and Alloys" 3rd Edition, pp. 309-312, CRC Press: Taylor & Francis Group, Boca Raton, FL, 2009.
32. "Ostwald Ripening" Image (Figure 5.3), Entegris: Particle Sizing Systems, 14 Aug. 2018, <http://pssnicomp.com/definitions/ostwald-ripening/>
33. "Layout of optical components in a basic TEM" Image (Figure 2.1), Wikipedia, Wikimedia Foundation, 14 Aug. 2018, https://en.wikipedia.org/wiki/Transmission_electron_microscopy
34. "Transmission Electron Microscope: A Basic Look at How TEMs Work", Azo Nano, 14 Aug 2018, <https://www.azonano.com/article.aspx?ArticleID=1723>.

* All TEM Images and Diffractions Patterns of the Cu-6 wt. % alloy disks are credited to Val Ouvarov-Bancelero, PhD. and recent graduate of the MSE program at UTA.

BIOGRAPHICAL INFORMATION

Kelly Claunch was born and raised in Fort Worth, Texas. She began her collegiate academic studies at Tarrant County College, initially focusing on mathematics and science courses due to her interest in these subjects. Upon transferring to The University of Texas at Arlington, Kelly began taking the courses required to complete a B.S. in Physics. It was along this journey that she discovered that a fast track program was available between the Physics/MSE departments at UTA. She took various MSE courses as an undergraduate and became interested in the field of materials science and engineering. After graduating with a B.S. in Physics from UTA in May of 2016, she began the M.S. program in the department of Material Science and Engineering at UTA in the Fall 2016 semester. Under the supervision of Dr. Choong-Un Kim, she worked on a variety of projects including the research presented in this paper.